


Topology-driven spatial organization of ring polymers under confinementDebarshi Mitra *, Shreerang Pande, and Apratim Chatterji *Department of Physics, IISER-Pune, Pune 411008, India* (Received 18 July 2022; accepted 12 October 2022; published 18 November 2022)

Entropic repulsion between DNA ring polymers under confinement is a key mechanism governing the spatial segregation of bacterial DNA before cell division. Here we establish that “internal” loops within a modified-ring polymer architecture enhance entropic repulsion between two overlapping polymers confined in a cylinder. Interestingly, they also induce entropy-driven spatial organization of polymer segments as seen *in vivo*. Here we design polymers of different architectures in our simulations by introducing a minimal number of cross-links between specific monomers along the ring-polymer contour. The cross-links are likely induced by various bridging proteins inside living cells. We investigate the segregation of two polymers with modified topologies confined in a cylinder, which initially had spatially overlapping configurations. This helps us to identify the architectures that lead to higher success rates of segregation. We also establish the mechanism that leads to localization of specific polymer segments. We use the blob model to provide a theoretical understanding of why certain architectures lead to enhanced entropic repulsive forces between the polymers. Lastly, we establish a correspondence between the organizational patterns of the chromosome of the *C. crescentus* bacterium and our results for a specifically designed polymer architecture. However, the principles outlined here pertaining to the organization of polymeric segments are applicable to both synthetic and biological polymers.

DOI: [10.1103/PhysRevE.106.054502](https://doi.org/10.1103/PhysRevE.106.054502)**I. INTRODUCTION**

Bacterial chromosomes are ring polymers, and just at the end of the replication process one can observe two partially segregated ring polymers conjoined at the specific point along their chain contour. The spatial segregation of these bacterial chromosomes occurs due to the entropic repulsion between them [1]. The hitherto established paradigm of bacterial chromosomes being considered as amorphous self-avoiding random-walk polymers without any internal organization within the cell has now been deemed obsolete [2]. In this vein, we have previously proposed that the *E. coli* chromosome can adopt particular polymer architectures aided by bridging proteins (and colocalization of *rrn* operons) to enhance the propensity for segregation due to entropic forces [3], as compared to the propensity of segregation in simple ring polymers under cylindrical confinement [1]. The proteins bridge different segments of the chain contour to create internal loops within the ring architecture of the *E. coli* chromosome [4–6]. These loops repel each other entropically and furthermore lead to an organization of genomic loci along the cell-long axis as seen in experiments [3].

These findings motivate us to perform a systematic study to identify the pool of polymer architectures that could increase entropic forces that drive segregation of the polymers in cylindrical confinement. Some of these polymer architectures may be adopted by bacterial chromosomes. We show that these modified polymer architectures could achieve localization of polymer segments, as has been observed *in vivo* for chromoso-

mal loci of two different bacterial species using fluorescence *in situ* hybridization (FISH) experiments [7,8]. Thus a detailed understanding of the generic principles pertaining to the role of modified-ring polymer architectures in the entropy-driven segregation, and consequently localization of polymer segments within cylindrical confinement, is imperative. This will help unearth the mechanisms of bacterial chromosome segregation in general.

It has been previously shown that the entropic repulsion between side loops situated along the backbone of a bottle-brush polymer leads to a spontaneous emergence of helical order under confinement [9]. Previous studies have also shown that two conjoined ring polymers spatially segregate spontaneously to maximize conformational entropy [1,10,11]. Flexible polymers are considered amorphous with the ability to adopt all possible conformations to maximize entropy. But we establish here that one can get segments of ring polymers with modified topologies to organize themselves along the long axis in cylindrical confinement. We create different polymer architectures with just two to four added cross-links (CLs) in ring polymers. This gives rise to internal loops (rings) within the ring polymer. This, in turn, results in mutual avoidance of loops within the cylinder and thus leads to localization of segments along the cylindrical axis. As a consequence, one observes the self-emergence of the internal organization of polymer segments within cylindrical confinement.

Furthermore, the presence of these internal loops within each modified ring polymer leads to the enhancement of entropic repulsion between two conjoined ring polymers. We also show that certain classes of looped architectures lead to greater enhancement of entropic forces than others. We

*Corresponding author: debarshi.mitra@students.iiserpune.ac.in

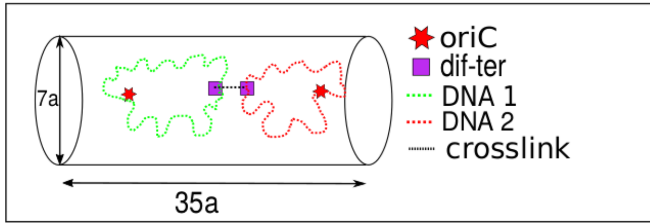


FIG. 1. A schematic representation of our simulation model: Two ring polymers (modified suitably with additional cross-links) of 500 monomers are confined within a cylinder. The two segments of each polymer chain labeled as *dif-ter* (following the convention for *E.coli* chromosomes), and represented by monomer index 250, have been cross-linked. This is inspired by the fact that newly replicated chromosomes in bacterial cells remained conjoined at the “ter” prior to cell division.

also outline the principles governing that enhancement. This mechanism of localization of polymer segments could lead to the localization of genomic loci in bacterial chromosomes, with relatively small fluctuations in positions along the cylinder long axis, as seen *in vivo*.

In this study, we model two replicated bacterial chromosomes as two bead spring ring polymers having 500 monomers each. We confine the polymers in a cylinder of appropriate dimensions to mimic the confinement imposed by the cell. Note that we do not model the process of replication, and we start our simulations with two overlapping ring polymers. In our model with 500 monomers, we label monomer-1 of each polymer as the *oricC*, and the 250th monomer in the ring polymer(s) is called the *dif-ter*. The two *dif-ter*s of the two ring polymers (with internal loops) remain cross-linked to each other by a spring throughout the simulation run. This is inspired by the case of bacterial chromosomes where the newly replicated daughter chromosomes remain conjoined at the *dif-ter* locus prior to cell division [1,10]; refer to Fig. 1 and Sec. II for more details. Later, we also modify the architecture of these ring polymers to further introduce loops within each ring polymer.

Thus, we present here a systematic analysis to elucidate general principles concerning the propensity of segregation and subsequent organization of two initially overlapping polymers for various architectures, which are under cylindrical confinement. We justify our computationally obtained observations for different architectures, with an analytic treatment of the Helmholtz free-energy difference between the overlapped and the segregated states, and we find that blob-theory-based calculations successfully explain our computational results. In addition, we also propose that a particularly designed polymer architecture is likely adopted by bacterial species *C.crescentus*. We posit that the cross-links that we introduce to modify the architectures may “effectively” arise in the *C.crescentus* chromosome due to the presence of proteins *in vivo* [2].

We have compared experimental Hi-C maps and FISH data with corresponding data obtained from our simulations. The Hi-C contact maps gives the probability of any two segments (monomers) of a DNA-polymer being in spatial proximity to each other. Hi-C data are obtained by averaging over many

cells, and they do not give the three-dimensional (3D) organization of loci within the cell, although it can be reconstructed from Hi-C maps [12–15].

On the other hand, FISH experiments are complementary in spirit to Hi-C experiments, in that they reveal the spatiotemporal distribution of a certain tagged locus (or a small number of tagged loci) within a particular cell.

Previous studies, which tried to reproduce contact maps of bacterial DNA, optimized a large number of constraints to find a detailed match with the experimental contact map [12–18]. We take an orthogonal approach and focus more on the mechanism underlying the spatial localization of loci in our study, and we try to match large-scale structures only. A detailed match would require a more detailed simulation model, which might not be particularly insightful to unearth general principles. Thereby, a detailed match is beyond the scope of this work.

We first give a brief overview of phenomenology of bacterial DNA segregation in Sec. II to provide context when we present our simulation model and results in Secs. III and IV, respectively. At the end of the Results section we describe the key insights we extract from our *in silico* studies. In Sec. V we extend our results to reconcile experimental observations pertaining to the organization of *C.crescentus* chromosome. We end the manuscript with the Discussion section, in which we summarize our work and mention avenues of further investigation.

II. BACTERIAL CHROMOSOMES

A. Basic background

The bacterium *C.crescentus* is a crescent-shaped cell, and the bacterium *E.coli* cell is a spherocylinder. We consider the cells of these bacteria to be cylindrical in shape, with diameter $\approx 1 \mu\text{m}$ and a length of $\approx 2 \mu\text{m}$. The chromosomes of *E.coli* and *C.crescentus* have 4.6 mega-base-pairs and 4 mega-base-pairs, respectively. Moreover, both are considered as model organisms to study chromosome organization.

In the *E.coli* and *C.crescentus* bacterial cells, certain genomic segments of the chromosome are localized around certain positions along the cell long axis, as observed in experiments [7,19]. Such localization patterns cannot be explained from entropic models of segregating ring polymers. We remind the reader that bacterial chromosomes are ring polymers, and the replication of mother DNA to create two daughter DNAs starts at a point called the *oriC*. The replication then proceeds bidirectionally along the two arms of the ring polymer and ends at the *dif-ter* loci. At the end of replication, the cell has two daughter DNA-ring-polymer chains.

For the *E.coli* cell, at the start of replication the *oriC* is at the midcell position [4,20–23]. Post replication, the DNA-polymer organization changes so that the *dif-ter* locus moves to the middle with the two *oriC* loci occupying the 1/4th and the 3/4th positions along the cell longitudinal axis. The two *dif-ter* loci of the two daughter DNA-polymer remain cross-linked until the time of cell division, which occurs a few minutes after replication is complete.

To ensure efficient segregation of initially overlapping DNA-polymer chains in cylindrical confinement, it is

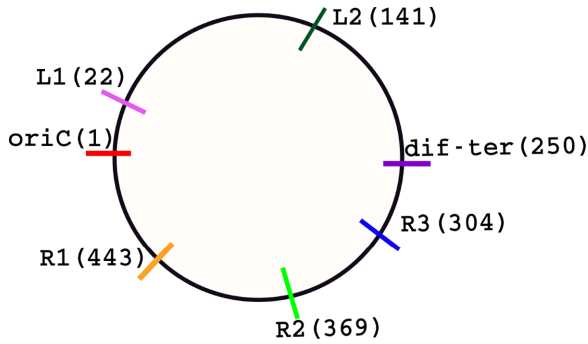


FIG. 2. The schematic shows the positions of the loci along the chromosome-polymer contour, which were fluorescently tagged in the experiments of Ref. [7]. These loci are *oriC*, L1, L2, R1, R2, R3, and *ter1*. The monomers corresponding to these loci are 1, 22, 141, 443, 369, 304, and 228, respectively, in our model of a ring polymer with 500 monomers. The spatiotemporal organization of the chromosome was inferred from the organization of these tagged loci. We thereby follow the monomers corresponding to the same loci (except *ter1*) in our simulations to infer the spatial organization of the chromosome-polymer. Instead of *ter1*, we follow the *dif-ter* locus, which is the 250th monomer and is close to *ter1*.

important that topological constraints are released. This is of the utmost importance since newly replicated chromosomes may be hindered from segregating due to topological constraints. The release of topological constraints in the case of bacterial chromosomes is accomplished by the presence of the enzyme DNA Topoisomerase (Topo II), which allows newly replicated daughter chromosomes to pass through each other akin to crossing of segments in phantom polymer chains [24–26]. Thus a comparative study investigating the role topological constraint release on the segregation mechanism of initially overlapping polymers under confinement is also in order.

Furthermore, detailed chromosomal contact maps obtained from Hi-C experiments [27] have unambiguously established the presence of topologically associated domains (TADs) for several bacterial chromosomes. The presence of macrodomains (spanning sections of $\sim Mbp$) within bacterial chromosomes has also been observed [27–29]. These may arise as a consequence of loops at specific positions in the genome [3]. These loops may be crucial to the formation of macrodomains and other characteristic features seen *in vivo* [3,5,30,31].

Previous FISH experiments on bacterial chromosomes, such as those reported in Refs. [3,7,19], involved the tagging of certain specific loci with fluorescent markers. The aim was to tag loci positions which were distributed over the entire ring contour, such that spatiotemporal information of different segments of the chain could be obtained. In our study, we plot the spatial distribution of the monomers corresponding to the same loci, which were chosen experimentally in [7] for *E.coli* chromosome, though we have access to the position distributions of all 500 monomers. The positions of these loci along the chain contour of a ring polymer can be seen in Fig. 2. The loci (monomers) are well-separated along the chain contour and therefore provide information on the spatial organization of the chromosome-polymer. The monomer

indices are shown in the schematic. We follow and present data for the spatial distribution for these same loci for all 12 polymer architectures. These polymer architectures have been classified into three different classes based on the orientation of the constituent loops with respect to the *dif-ter* cross-link.

When we map a particular architecture to the DNA of a particular bacteria, we can analyze the spatial distribution of any monomer corresponding to any particular locus that we need to. Thus, we chose to track different monomers from what is shown in Fig. 2, when we compare our data from simulations to spatial distributions of loci of *C.crescentus*, as provided by experiments.

B. Unresolved questions

Through this work, we aspire to address the following unresolved questions:

(i) It is already known that a branched topology leads to a higher propensity of the spatial segregation of two initially overlapping, confined polymers [10]. Do some classes of topologies (architectures) induce higher entropic forces of segregation than others?

(ii) Once the two initially overlapping polymers (daughter chromosomes) demix spatially, it is imperative that they stay demixed before cell division occurs *in vivo*. Are there certain classes of architecture that have a greater propensity of remaining demixed after they have spatially segregated?

(iii) In an earlier work [3] we have shown that a particular polymer architecture leads to the localization of certain polymer segments as seen *in vivo* in the *E.coli* chromosome. The localization of these segments arises due to the entropic repulsion between the constituent loops. Can other architectures lead to the localization of these polymer segments to other specific regions along the cylindrical long axis? Thereby, can we design loops *a priori* along the chain contour using intuition to obtain localization of specific segments, which can then be matched to experimental data for other bacterial chromosomes?

(iv) Can the induced forces of entropic segregation in the case of different architectures be calculated and justified analytically? Are these calculations (done for idealized systems) consistent with simulation data that measure the propensity of polymer segregation?

(v) In the different classes of architectures that we study, what is the organization of the constituent loops along the cylindrical axis? How does the organization of the constituent loops vary for architectures of different classes?

III. SIMULATION MODEL AND METHODS

We perform Monte Carlo simulations using a bead spring model of two flexible ring polymers with 500 monomers in each chain. We introduce additional cross-links to obtain polymers of different architectures. If there are N monomers in the simulation, each MCS involves N attempts to displace a monomer in a random direction. The attempt may or may not be accepted as per the Metropolis criterion. When attempting a random displacement, the monomer should be chosen at random from N monomers.

Two neighboring monomers (beads) along the chain contour interact via the harmonic spring potential with

energy $V_H = \kappa(r - a)^2$, where r is the distance between the monomers. The unit of length in our study is a , where $a = 1$ is the equilibrium length of the harmonic springs between two neighboring monomers. The spring constant κ is $100k_B T/a^2$. The excluded volume (EV) interactions between monomers are modeled by the Weeks-Chandler-Anderson (WCA) potential, and the diameter of each monomer is given by $\sigma = 0.8a$. The form of the WCA potential is

$$V_{\text{WCA}} = 4\epsilon[(\sigma/r)^{12} - (\sigma/r)^6] + \epsilon_0, \quad \forall r < 2^{1/6}\sigma. \quad (1)$$

The quantity ϵ_0 is needed to ensure that the potential goes smoothly to zero at the cutoff, and $V_{\text{WCA}} = 0$ for values of r greater than the cutoff. Note that the 250th monomers of the two polymers have a cross-link (CL) between them. This is inspired by the case of bacterial chromosomes where the newly replicated daughter chromosomes remain conjoined at the *dif-ter* locus prior to cell division [1,10]; refer to Fig. 1 and Sec. II for more details. The polymers are confined to a cylinder with appropriately chosen dimensions.

A. Dimensions of cylindrical confinement

We confine two ring polymers within a cylinder of radius $3.5a$ and a length of $L = 35a$; refer to Fig. 1. This ensures an aspect ratio of 1 : 5. This aspect ratio is observed *in vivo* for an *E.coli* cell in slow growth conditions [32] with two daughter chromosomes at the end of the replication process and just before cell division. This particular choice of parameter results in a colloidal volume fraction of monomers of 0.2. We consider the walls of the cylinder to be hard (with infinite potential) such that we reject any Monte Carlo trial move in which a monomer center attempts to occupy a position located outside the cylinder. The dimensions of the confining cylinder correspond to the volume accessible to the center of the monomers.

If we think that the polymer chains represent replicated *E.coli* daughter chromosomes, and since the *E.coli* chromosome has 4.6 Mbp of DNA, each monomer corresponds to 9.2 kbp of DNA. Note that the Kuhn length of bare ds-DNA is known to be 100 nm with approximately 300 base pairs (bp). Thus each monomer corresponds to a lengthscale much greater than the Kuhn length bare DNA. However, it is known that ds-DNA is compacted by histone like HU proteins in bacteria. Since the *E.coli* cell has a diameter $1 \mu\text{m}$, which is $7a$ in our simulations, we may consider $a = 150$ nm in real units. We do not consider larger cylinders as it is established that segregation occurs only when the radius of the confining cylinder is less than the radius of gyration R_g of the polymer [1].

We confine the polymers in a cylinder instead of a spherocylinder, though it is known that the shape of an *E.coli* cell is closer to that of a spherocylinder. However, in this manuscript we just want to establish the principles of organization of polymers having different architectures subjected to cylindrical confinement, without any loss of generality of whether the polymer is a synthetic polymer or the chromosomes of other rod-shaped bacterial cells.

B. Initializing and equilibrating the system

As polymers spontaneously segregate due to EV interactions, we equilibrate the system of two ring polymers in an initial mixed state by the following procedure. We introduce the monomers at random positions in the cylinder and allow the chain to diffuse freely *without* excluded volume interactions between monomers. However, the harmonic spring interactions are present (including the additional cross-links). We run the simulation for 10^6 MCS to equilibrate. Since we initialize monomers randomly within the cylinder, neighboring monomers along the chain contour can be initially far away. Thus at the start of the simulation, the springs between such monomers may be highly stretched. But with the start of the simulation, the monomers rapidly move towards each other, and the springs reach lengths close to their equilibrium values much before 10^5 MCSs. Once the chains get completely “mixed” spatially, we switch on the excluded volume interactions and study the segregation dynamics of the two polymers.

Due to the initialization procedure, concatenations between loops (topological entanglements) can get introduced. When we incorporate the effect of topoisomerase (i.e., periodic shrinking of monomers), then these concatenations have suitable opportunities to get released over the length of the simulation runs. The procedure for the same is discussed in the subsequent section. However, for the case in which we do not incorporate this topological constraint release mechanism (relevant for synthetic polymers), these topological links could prevent segregation and thus reduce success rates of segregation. From a biological point of view, if the two polymers are considered to be newly replicated chromosomes, then it is not unlikely that the two DNA-polymers would be topologically linked just after replication. Hence, for studying such scenarios, the initialization procedure employed by us is apt. For future studies of segregation properties with synthetic polymers, it will be more apt to initialize the system such that there are no concatenations between the two polymers.

Furthermore, in this study we use the WCA potential instead of a hard-sphere potential, to ensure that there are no spatial overlaps between monomers. The reason for this has been elaborated upon in Sec. I of the supplementary information (SI) [33].

C. Release of topological constraints

In addition to studying nonliving polymers in which chains do not cross each other, we also consider polymer chains that can pass through each other at regular intervals to release topological constraints. This is done to mimic the effect of Topoisomerase in the *E.coli* cells (*and other bacterial cells*), which allows release of topological constraints by facilitating chain crossing. To implement this, we reduce the σ to $\sigma' = 0.2a$ after every 10 000 MCS. We let the system evolve using Monte Carlo trial moves with $\sigma = 0.2a$ for the subsequent 900 MCS to allow the release of topological constraints, before reverting to $\sigma = 0.8a$. Note that we allow chain crossing infrequently for only about 10% of the total duration of the simulation, as excluded volume interactions are important for entropic repulsion between loops, which drives segregation. If the duration of topological constraint release is increased

TABLE I. The table lists the monomer indices that have been cross-linked to obtain architectures as shown in Fig. 3. The monomer pairs that are cross-linked are given in parentheses.

Architecture	Pairs of cross-linked monomers
Arc-0	no additional CL
Arc-2	(125,1), (375,1)
Arc-2-2	(125,1) (375,1) (156,218) (282,344)
Arc-3	(125,1)
Arc-4	(200,50)
Arc-6	(150,230) (350,270)
Arc-7	(20,100) (400,480)
Arc-8	(100,1) (125,200) (200,300) (375,300)
Arc-9	(125,1) (125,375) (187,312)
Arc-10	(20,100) (480,400) (187,313)
Arc-11	(125,1), (187,313)

significantly, then the entropic repulsion is significantly reduced, and if the duration is significantly reduced, then segregation of overlapping polymers is prevented by the presence of topological constraints.

Though this is a convenient simulation strategy to release topological constraints all at once for all chain segments and is also computationally cheap, this is unlikely to mimic the real dynamics within the cell. However, the “equilibrium organization” of chromosomes and the localization of loci (which will be established subsequently in this study) is likely to be unaffected by this choice since it only affects the dynamical aspects. Secondly, even though the action of Topoisomerase might produce qualitatively different results with regard to the dynamics, here we choose to focus on whether a particular architecture leads to a higher success rate of segregation than others in the presence of a topological constraint release mechanism. Incorporating a more detailed model of the action of the Topoisomerase enzyme is outside the scope of our current work.

D. Modifying the ring-polymer architecture

We modify a ring polymer suitably to obtain different polymer architectures by introducing harmonic spring interactions between monomer pairs at specific sites along the chain contour. Thus we cross-link specific monomers along a chain contour. The spring constants corresponding to the additional cross-links are given by $\kappa = 100k_B T/a^2$, and the springs have an equilibrium length of a . This results in a variety of looped structure of the polymers. We keep a minimal set of additional cross-links and ensure that we do not introduce more than four additional cross-links. In Table I we list the sites of cross-links by which we generate different polymer architectures, as listed in Fig. 3. The considered polymer architectures represent a variety of looped structures, and the sizes of the loops vary from 60 to 130 monomers.

E. Classification of looped architectures

We start with a ring polymer, which we label Arc-0. We then introduce a single cross-link and create two internal loops to create Arc-3 and Arc-4. In Arc-3 and Arc-4, the smaller

loop (with 125 monomers) is placed differently with respect to the bigger loop with 375 monomers. In the two architectures, the position of the smaller loop is at different contour lengths away from the *dif-ter* monomer, which is cross-linked to the *dif-ter* of the second ring polymer; refer to Figs. 1 and 3.

We represent Arc-3 as having a “linear” looped architecture where the two loops are schematically placed linearly along the cylindrical axis provided the axis is long enough (not shown). Arc-4, on the contrary, has a “side loop” architecture. This distinction is being made based on how the loops are arranged with respect to the *dif-ter* cross-link. This enables us to study the effect of loop orientation on the organization and segregation of spatially confined polymers. The nomenclature will be justified when we present data on the overlap of monomers from different loops.

To study the effect of additional loops, we design architectures with three loops where these loops are oriented in different ways. In Arc-5 and Arc-11 the loops are placed linearly along the cylindrical axis, whereas in Arc-6 and Arc-7 we have two additional “side loops.” We have also designed Arc-6 and Arc-7 such that they have loops of the same size, but in Arc-6 these loops are closer to the *dif-ter* cross-link whereas in Arc-7 the loops are located close to the *oriC* along the chain contour. We shall establish significantly that this leads to key differences in the propensity for entropic segregation for two overlapping polymers having these architectures.

We also design a number of polymer architectures that employ both “linear” as well as “side” loops. Such architectures are termed as hybrid architectures, and they may also have two, three, or four additional loops. This gives rise to the architectures Arc-2, Arc-2-2, Arc-8, Arc-9, and Arc-10. We will establish later that some of these hybrid architectures lead to distinct localization patterns of genomic loci, while certain other architectures lead to high propensities of entropic segregation.

The nomenclature of Arc-0, Arc-2, and Arc-2-2 has been borrowed from the nomenclature used in [3], where we used these architectures to explain localization data of loci for the *E.coli* chromosome. In our previous work, we had explicitly modeled replication, and the loop sizes for Arc-2-2 were slightly different from that presented in this work. That resulted in a better match with Hi-C data of *E.coli* chromosomes. The other architectures investigated in this work were designed thereafter.

F. Importance of the ‘ter’ cross-link

The terminology “side loops” and “linear loops” can assume significance only because of the presence of the *dif-ter* cross-link between the two initially overlapping ring polymers. This restricts the number of conformations accessible to the two polymers. For instance, Arc-3 and Arc-4 are not equivalent architectures only due to the presence of the *ter* cross-link.

G. Quantifying the organization of specific polymer segments (tagged genomic loci)

To establish the organization of the polymers along the cylindrical long axis, we plot the probability distributions of

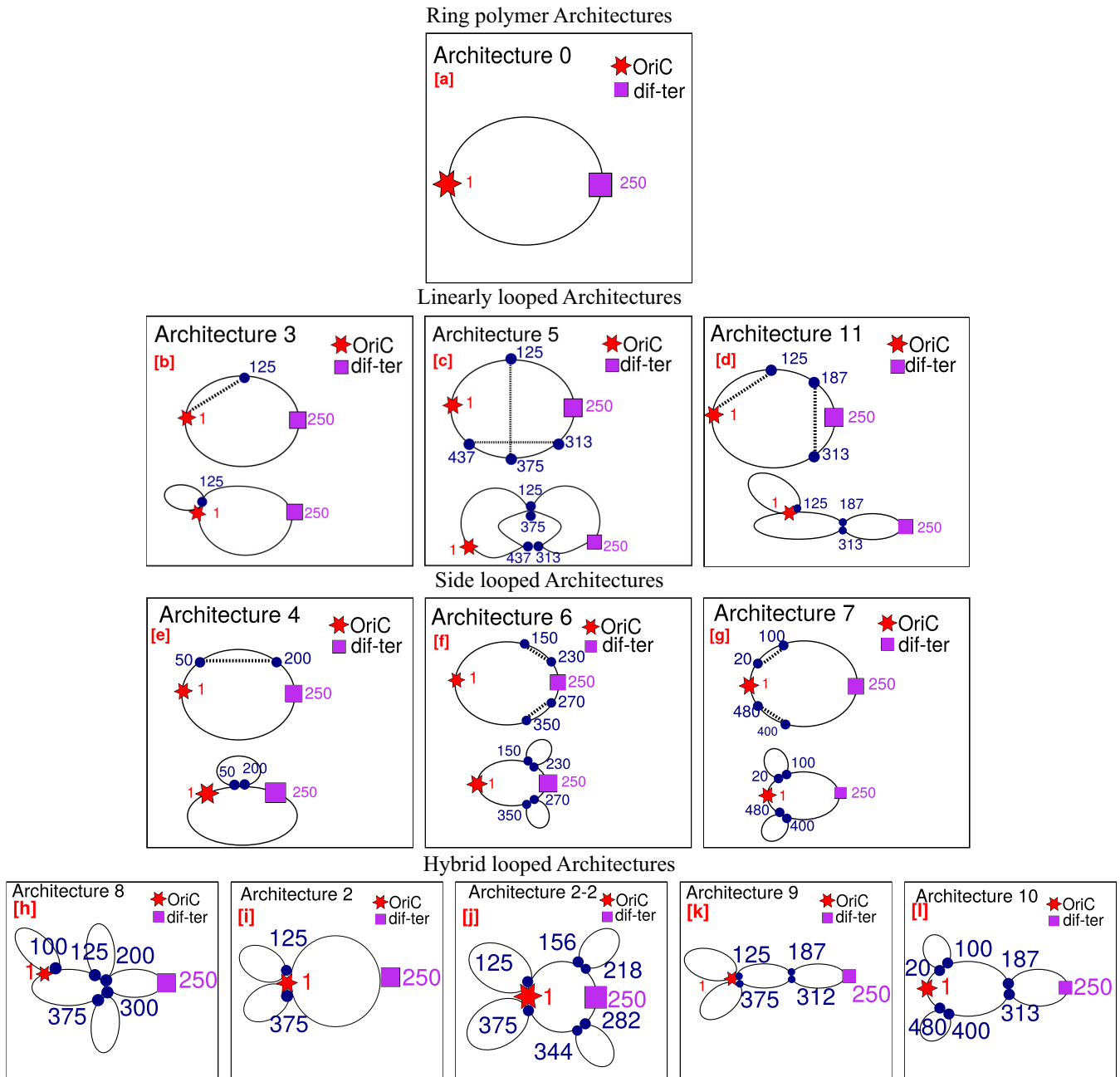


FIG. 3. Schematic representation of polymer architectures. We have classified all the polymer architectures according to our design of loops along the chain contour; refer to Sec. III D. Each polymer of a particular architecture is cross-linked at *dif-ter* to another identical polymer (refer to Fig. 1). The dashed lines refer to the introduced springs between specific monomers (indices marked in blue) in the ring architecture to create the additional loops. With respect to the *dif-ter* position, the Arc-3 polymer has loops placed along a line along the cell long axis, and it is therefore called “linearly looped” architecture. We will see later that the monomers of different loops (statistically) occupy different sections of the cylinder along the long axis for the Arc-3 polymer. On the other hand, the Arc-4 architecture has a small “side loop”; we shall see that the monomers of the big loop and side loop overlap significantly. We introduce additional loops, with different orientations of loops to create Arc-5, Arc-11, Arc-6, and Arc-7. Finally, we also have architectures having a combination of both “side loops” and “linear loops,” referred to as “hybrid” architectures.

the position along the cylindrical long axis of certain specific monomers. We calculate this distribution after the initially overlapping polymers have segregated to two halves of the cylinder. The chosen monomers are fairly equally spaced along the chain contour and hence reliably indicate the degree

of (linear) organization along the cylindrical axis. We study the spatial localization of monomers: 1, 22, 141, 443, 369, 304, and 250 in each of the two polymer chains. If the two polymer chains are thought of as being analogous to newly replicated chromosomes in *E.coli* cells, then the positions of

these monomers along the contour correspond to loci labeled as *oriC*, L1, L2, R1, R2, R3, and *dif-ter* in [3,7]: refer to the schematic in Fig. 2.

H. Modeling the *C. crescentus* bacterial species

We find that the confined polymer with a specially designed architecture successfully organizes the polymer segments in a way that is particularly relevant for *C. crescentus*. Note that now each monomer represents 8 kbp of DNA, as the chromosome has 4 Mbp. In the *C. crescentus* chromosome, the *ori* remains tethered to the pole *in vivo* [19]. In our simulation model for *C. crescentus*, the monomer index 22 corresponds to the *ori*, which we tether to one of the cylinder (cell) pole *via* a harmonic potential, with a spring constant $1k_B T/a^2$. We also look at the spatial distributions of other loci such as *pilA*, *pleC*, *podJ*, and *ter* [2]. These loci correspond to the monomer indices 122, 182, 238, and 272, respectively. When we apply the results of our studies for a particular architecture to understand the chromosomal organization of *C. crescentus*, then we cross-link the 272th monomer of each of the two chains, refer to Fig. 1, as that monomer represents the *dif-ter* position for *C. crescentus*. We also look at the contact map obtained from our simulation model using the procedure outlined in [3].

I. Choice of Monte Carlo simulation technique

We conduct our studies on the effects of architecture on the success rates of segregation of initially overlapping polymers in confinement and subsequent localization using Monte Carlo (MC) simulations. It has been shown previously [34,35] that Monte Carlo simulations successfully reproduce diffusive dynamics of particles at a coarse-grained level as the polymers segregate. Thus Monte Carlo simulations have been used widely in studies on phase separation kinetics [36] and polymer dynamics [37,38]. We emphasize that we have sufficiently low volume fractions to capture diffusive dynamics of polymers.

Furthermore, we employ MC for this study since it allows us to reduce the bead size of the beads in our bead spring model at infrequent intervals. We do this to mimic the effect of the Topoisomerase enzyme. Note that this cannot be done in the usual Langevin (or Brownian dynamics) simulations as it would lead to discontinuities in potentials and infinite forces. Note that the incorporation of topological constraint release implies that the study is intrinsically a nonequilibrium system in which detailed balance is violated. In this case, the Monte Carlo step displacement of monomers in the chain captures the local diffusive dynamics in the confined cylinder, and the subsequent exploration of phase space.

IV. RESULTS

A. Segregation propensity of polymer architectures

We first present a comparison of segregation success rates of two spatially overlapping polymers, for each of the different polymer architectures. In each case, the two overlapping polymers have identical architectures. We study the phenomenon in the absence of topological constraint release as in

synthetic polymers, as well as when we introduce topological constraint release to mimic DNA-polymers.

To estimate the segregation success rates for a particular architecture, we give 50 independent runs each starting from a different initially overlapped configuration of polymers. In each run, we measure the distance D_{com} between the centers of mass of the two polymers from the start of the simulations, i.e., when we switch on EV interactions between monomers after equilibration. If the mean distance $\langle D_{\text{com}} \rangle$ is $\geq d_T$, where d_T is the designated threshold value, we deem the polymers to have segregated. We chose $d_T = 0.48L$, and $\langle D_{\text{com}} \rangle$ is calculated over 4×10^7 MCS postsegregation. This implies that the two polymers occupy different halves of the cylinder.

In Figs. 4(a)–4(c), we show the evolution of the values of D_{com} with MCSs, starting from relatively low values (when polymers are in an overlapped configuration) to higher values for three different independent runs, respectively. We compare data for Arc-0 architecture with those for Arc-2 architecture. We have intentionally shown data where the polymer is unable to fully segregate, so that the reader can directly envisage how D_{com} fluctuates for the cases with unsuccessful segregation. The D_{com} -MCS data for all 50 runs are given in Fig. S1 of the SI [33].

Similar sets of 50 runs were given for each of the 11 architectures considered in this study. Thereafter, in Fig. 4(d) we show the segregation success percentage and the mean number of MCS required for successful segregation (N_{MCS}) for different architectures, for the studies where chain crossing is disallowed. On the left y-axis we show the success rates of segregation, which indicates the percentage of independent runs that result in a segregated configuration of the polymers. The right axis shows variation of N_{MCS} for the different architectures.

We compare the data presented in Figs. 4(d) with 4(e), where we consider all architectures with chain crossing introduced. We observe that the ring polymer architecture Arc-0 has low segregation success rates in both studies. When chain crossing is allowed, the rates of successful segregation increase slightly for the Arc-0 architecture, as we see in Fig. 4(e). We checked that for shorter polymers with 100 monomers, the polymers nearly always segregate even without release of topological constraints, as seen in previous studies [39].

From Fig. 4(d) [and Fig. 4(e)], we further note that Arc-4 shows a higher success rate of segregation as compared to that of Arc-3. We remind the reader that both Arc-3 and Arc-4 have one additional loop each, but the loops in the two cases are oriented differently with respect to the *ter* cross-link. However, the linearly looped architectures Arc-5 and Arc-11 (with two additional loops) have higher success rates of segregation, as compared to that of Arc-6 and Arc-7, which are side-looped architectures. Arc-6 and Arc-7 also have two additional loops each, of identical sizes but positioned differently with respect to the *ter*-CL. Interestingly, we note that Arc-6 shows a higher success rate of segregation as compared to Arc-7. Note that for both of these architectures we have two additional side loops, but in Arc-6 the loops are closer to the *dif-ter* CL, whereas in Arc-7 the loops are located closer to the *oriC*. We reconcile these observations with further analysis presented subsequently in the text.

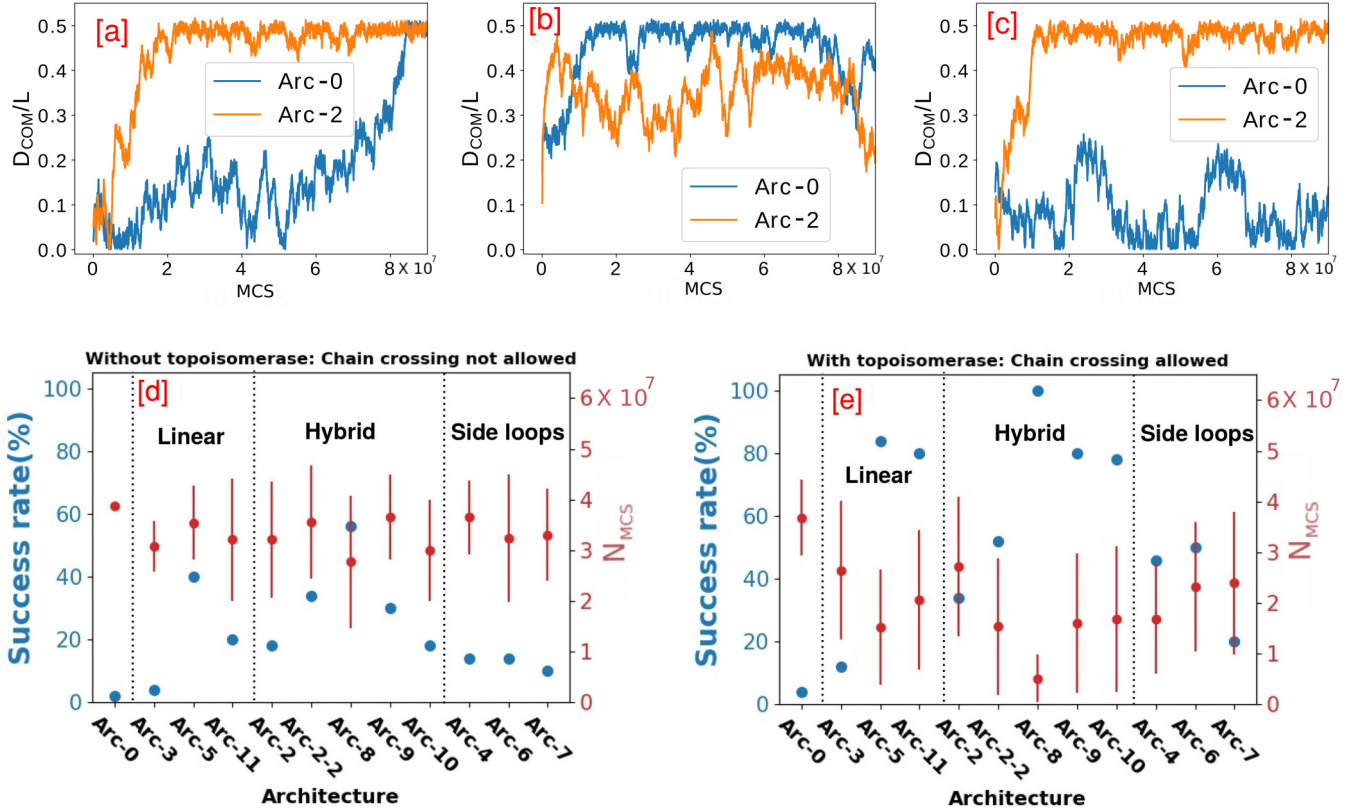


FIG. 4. Success rates of segregation of overlapping polymers for different architectures: Subfigures (a)–(c) show the distance between the center of masses D_{com} vs MCS of the two initially overlapping polymers as they undergo segregation in the Monte Carlo simulation for three independent runs for the Arc-0 (ring polymer) and Arc-2 architectures. Runs for which D_{com}/L fluctuates significantly below 0.5 are deemed as runs that did not lead to successful segregation. Chain crossing is allowed at designated rates (refer to the text) for the data presented in subfigures (a)–(c). The subfigures (d) and (e) show a comparison of success rates of segregation for different architectures, which indicates the percentages of independent runs that lead to segregation. We compute this by counting the number of runs that show successful segregation from a pool of 50 independent runs for each architecture. The right y-axis shows the mean number of MCS required for segregation (N_{MCS}). The error bars have been computed using the data from the successfully segregated cases from the entire set of 50 runs. We note that the architectures with additional cross-links lead to lower values of N_{MCS} and higher success rates of segregation, as compared to that of a ring polymer (Arc-0). The effect of topological constraint release has not been incorporated in (d), while release of topological constraints is allowed in (e).

For results similar to Figs. 4(d) and 4(e), but with a different criterion for identifying the success of segregation with a different value of the threshold d_r , refer to Fig. S2 in the SI [33].

In Fig. S3 of the SI [33], we also present data with different averaging criteria to calculate $\langle D_{\text{com}} \rangle$. We find that the qualitative trends discussed above in Figs. 4(d) and 4(e) *vis-a-vis* different architectures remain unchanged for these studies as well. However, quantitatively the success rates of segregation (for all architectures) may vary if different criteria to compute the success rates of segregation are chosen. For bacterial chromosomes it is imperative that the two chromosome fully segregate spatially before cell division, thereby we present data with more stringent criteria for segregation in the main paper.

Effect of topological constraint release: We also observe that release of topological constraints leads to increased success rates of segregation and fewer MCS required for spatial segregation (N_{MCS}). For the data presented in Fig. 4(d), we do

not allow the release of topological constraints by a suitable decrease of the monomer diameter at regular intervals. We also note that even for the architectures that successfully show segregation, N_{MCS} is much lower when topological constraints are released, as seen in Fig. 4(e). Thus the release of topological constraints is pivotal to accomplish timely and efficient segregation of spatially overlapping polymers, as in bacterial chromosomes.

B. Propensity of segregated polymers to overlap

After the initially overlapping polymers “demix” due to entropic conditions, could some architectures again get spatially overlapped to some degree due to thermal fluctuations? This is crucial as segregated chromosomes need to remain well-segregated with minimal overlap before cell division takes place. To investigate this, we look at the probability distributions $P(D_{\text{com}})$ of the distance between the centers of mass of the two polymers D_{com} for each of the architectures; refer to

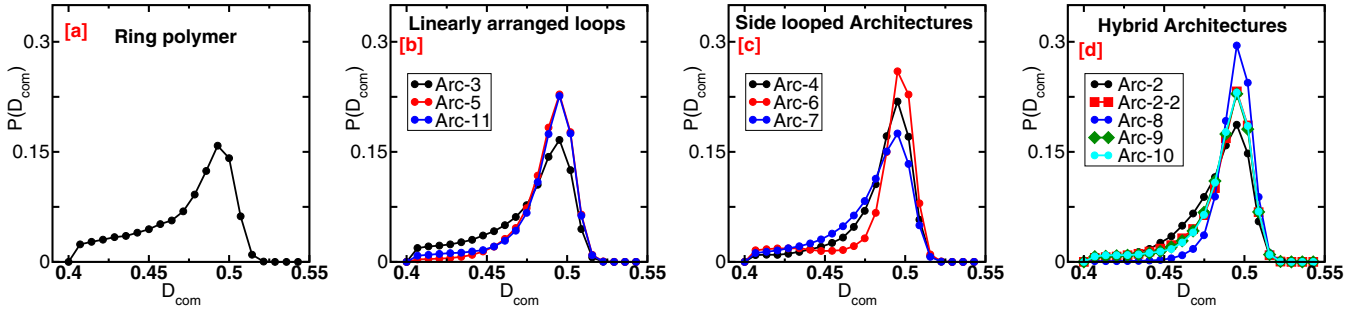


FIG. 5. Propensity of the two polymers to overlap postsegregation: A pair of segregated polymers might subsequently overlap spatially due to thermal fluctuations. We investigate whether particular polymer architectures disfavor spatial overlap between the pair of segregated polymers. We show the probability distribution $P(D_{\text{com}})$ of the distance between the centers of mass (D_{com}) of two polymers computed from 50 independent runs for different architectures in the subfigures. We calculate these distributions from only those microstates for which $D_{\text{com}} \geq 0.4L$. Thereby, the number of microstates over which these distributions have been computed varies across architectures. For the ring polymer, the success rate of segregation is low, and hence fewer microstates have been used to calculate $P(D_{\text{com}})$. The x -axis has been scaled by the cylinder length L . Data are collected every 30 000 MCS over 9×10^7 MCS. Since two polymers are deemed segregated if $\langle D_{\text{com}} \rangle \leq 0.48L$, nonzero $P(D_{\text{com}})$ at $D_{\text{com}} < 0.48L$ is indicative of the presence of overlaps. Chain crossing is allowed for the data presented.

Figs. 5(a) and 5(d). The distribution has been computed using those microstates for which $D_{\text{com}} \geq 0.4L$. We observe that the Arc-0 (ring polymer) shows a relatively broad distribution as compared to other architectures. This indicates that a pair of polymers (chromosomes) with the Arc-0 architecture has significant overlap even after segregation. We also note that Arc-8 with three “side loops” shows the highest propensity to avoid spatial overlap as $P(D_{\text{com}})$ is sharply peaked near $D_{\text{com}} = 0.5L$. We note that Arc-6 shows a narrower distribution as compared to Arc-7, while Arc-4 shows a narrower distribution as compared to Arc-3. We establish the underlying mechanism for these observations subsequently in the text.

The probability distributions shown in Fig. 5 are indicative of the free energy of polymer configurations with different degrees of overlap (and corresponding D_{com}) for different architectures. Note that the free energies corresponding to different values of D_{com} can be found from the probability distributions since the free energy can be expressed as $F(D_{\text{com}}) = -k_B T \ln[P(D_{\text{com}})]$.

C. Spatial organization of polymer segments: Tracked by localization of genomic loci

After the two polymers have segregated to two halves of the cylinder starting from a mixed configuration, we investigate specific organization in the polymers due to the presence of internal loops. We plot the spatial probability distribution of a few chosen monomers along the chain contour along the cylindrical long-axis for different architectures; refer to Sec. III. In Figs. 6 and 7, we show the distribution of the position of loci along the cylinder long-axis. To plot these distributions, we consider microstates from only the successfully segregated cases. For this analysis, we have incorporated the effects of Topoisomerase. Note that we show the spatial distribution of only one of the *dif-ter* loci since the two *dif-ter* loci are cross-linked, and have nearly identical distributions. But for other loci, we plot the probability distribution such that it reflects the spatial distribution of the pair of loci from the pair of polymers.

In Figs. S4–S9 of the SI [33], we show similar data but without incorporating the effects of chain crossing. We note that the effect of chain crossing does not significantly affect the localization of the loci. Different monomers (genomic loci) get localized in some architectures due to the presence of internal loops. There the constituent loops of each architecture entropically repel each other and thus specific monomers or loci get localized to specific regions along the cylinder long axis.

In data presented in Figs. 6 and 7, we can develop intuition to infer the positions where these loci get localized along the cylindrical long-axis due to the entropic repulsion between the constituent loops. In some architectures, such as Arc-0, we do not observe the localization of the loci. We discuss in detail the localization properties of all the loci for a few architectures. Similar intuition can be extended for the other architectures to understand the localization properties (or lack of localization).

Arc-3: For a study with a pair of segregated polymers with Arc-3 architecture, the localization of *dif-ter* is automatically achieved due to the *ter*-cross-link coupled with the strong mutual entropic repulsion of the two large loops which span 126 – 250 – 375 – 499 of each ring-polymer. The smaller loop (spanning monomers from 1 to 125) of each ring polymer tries to avoid the larger loop and thereby is found near the poles. But the *oriC* forms the junction between the two loops, and hence the peak of its probability distribution is slightly shifted from the poles. When the *oriC* is located at the poles (in some microstates due to statistical fluctuation), then the loops of the polymers will spatially overlap with each other, which will be entropically disfavored. Thus, the positions closest to the poles are preferentially occupied by locus L1 (monomer 22), which is part of the smaller loop. Locus R3 (monomer index 304) remains relatively close to the *dif-ter* while avoiding the monomers of the smaller loop, thereby the probability of finding it is higher close to the center of the cylinder.

On the other hand, R1 (monomer index 443) is part of the bigger loop and close to *oriC*. Thereby, it remains relatively delocalized though it avoids polymer segments closer to

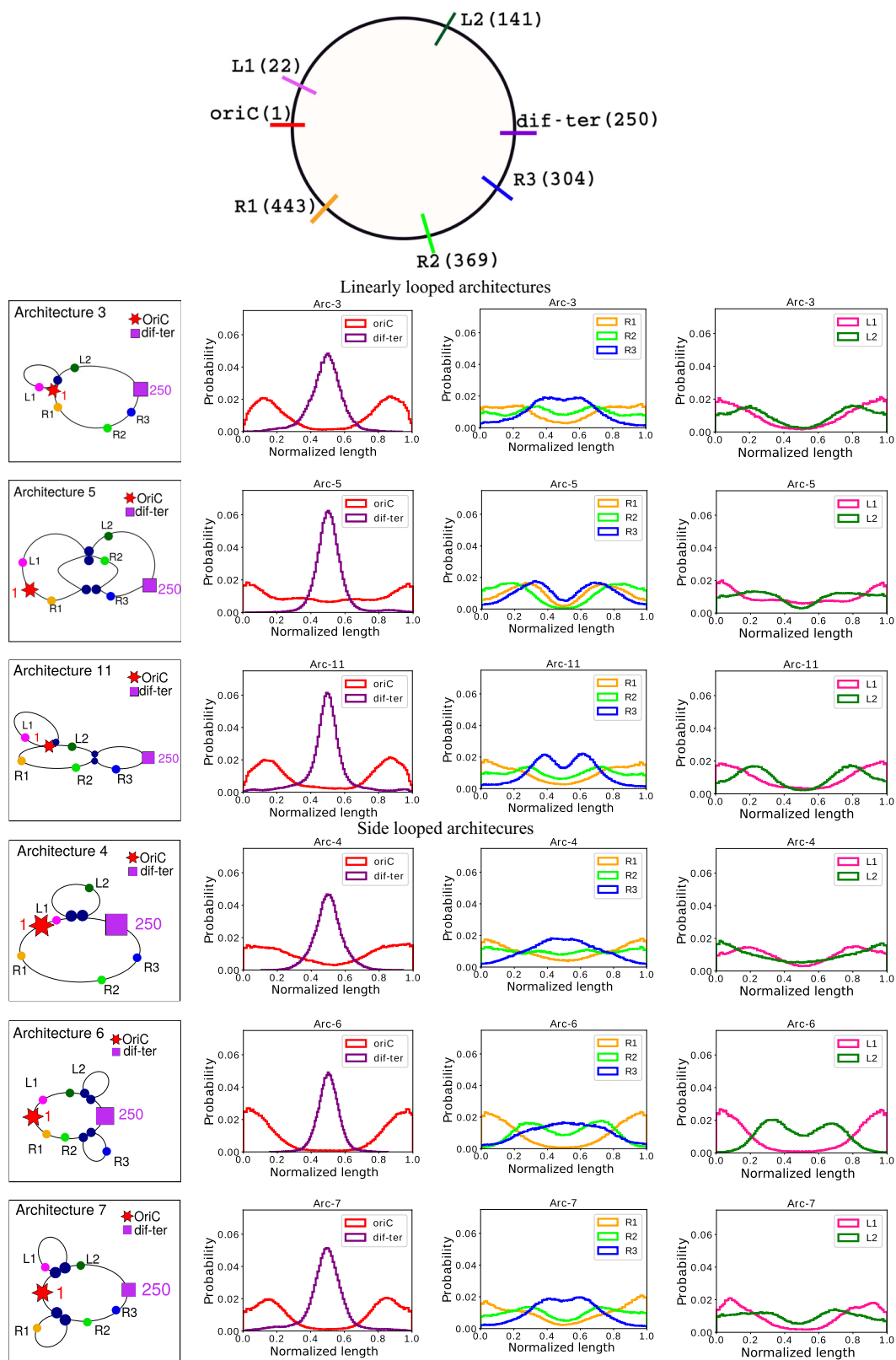


FIG. 6. Localization of specific chosen monomers (genomic loci): The figure shows the spatial distribution of the *oriCs* and the other loci for linearly looped architectures and the side looped architectures. At the top we show a schematic of the chromosome contour with the loci and the corresponding monomer indices marked along the chain contour. Each row corresponds to the probability distribution of positions of tagged monomers for a particular architecture. There is also a schematic of the architecture with the loci marked, provided for aid of interpretation of corresponding localization data. We allow chain crossing at the rates specified in Sec. III.

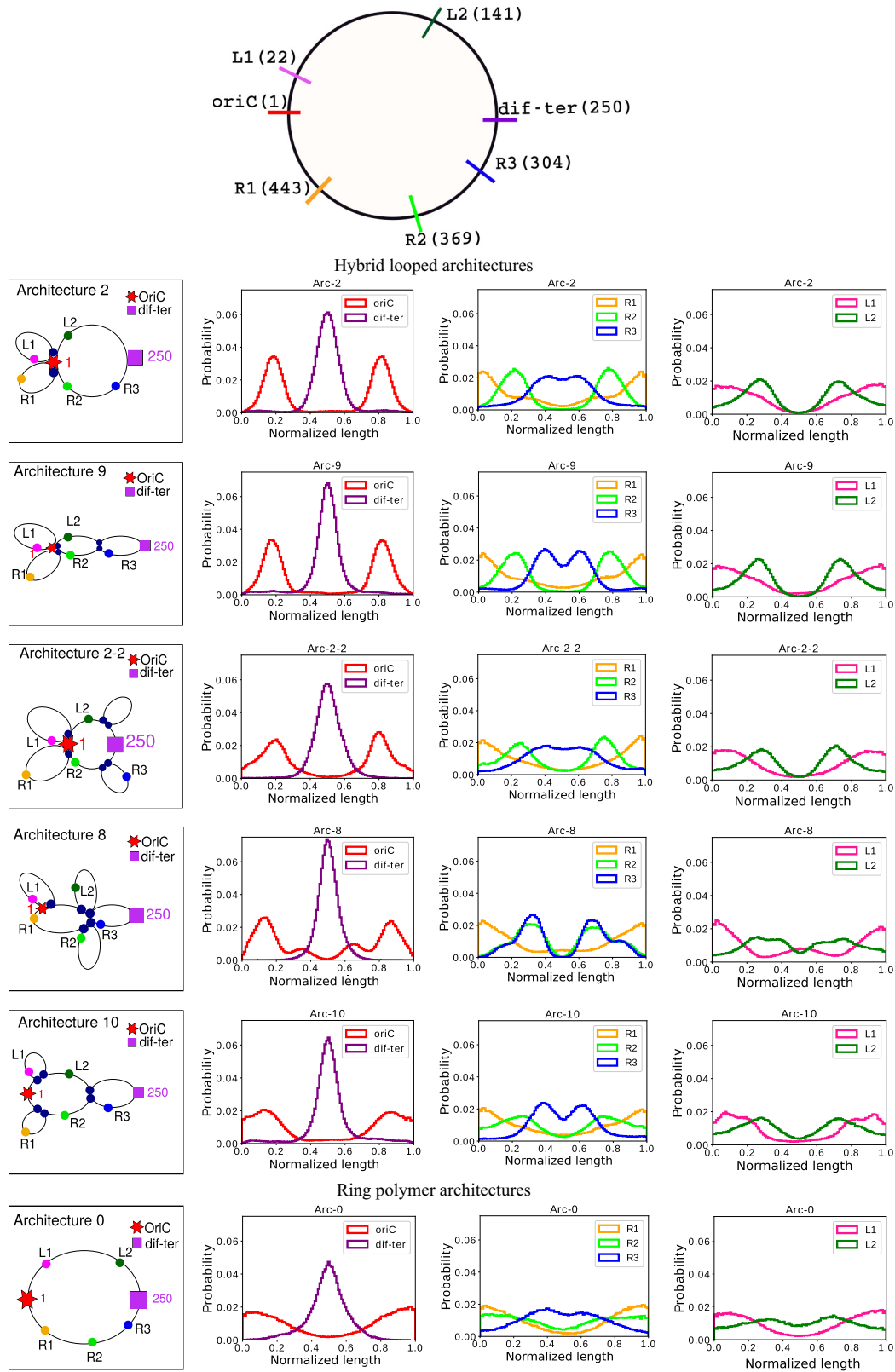


FIG. 7. Localization of chosen monomers (genomic loci) for some architectures: The figure shows the spatial distribution of the *oriC*'s and the other loci for hybrid architectures. At the top we show a schematic of the chromosome contour with the loci and the corresponding monomer indices marked along the chain contour. Other details are identical to that in the figure caption of Fig. 6.

dif-ter, while having a slightly higher propensity to be found near the *oriC*. Locus R2 (monomer 369) is most delocalized and attempts to avoid the segments near *oriC* as well as segments near *dif-ter* and shows a small peak. Note that R2 is located at the midpoint of the right arm of the ring polymer. Thereby, it is relatively unhindered from exploring different regions along the long-axis. Locus L2 (monomer 142) is near the cross-link between monomer pairs 1 and 125, and it has a distribution closer to the *oriC* distribution.

Arc-5: The Arc-5 architecture is comprised of three loops placed linearly along the cell long axis. The middle loop has 124 monomers, while the two outer loops have 188 monomers each. Furthermore, the loci R1, R2, R3, and L2 are located close to the cross-links positions i.e., near the junction of the loops. For two segregated polymers with Arc-5 architecture, the monomers of the smaller loop in the middle get entropically repelled by monomers of the two larger loops on its two sides, and thereby they occupy the regions around the quarter positions along the long axis. Hence, R1, R2, R3, and L2 are found near the quarter positions with a higher probability. The monomers around R2 and R3 avoid each other, thus the distribution peak for R3 is closer to the location of *dif-ter*. As always, the *dif-ter* is localized near the center of the cylindrical long axis, due to the repulsion between loops from two different polymers. The loci *oriC* and L1 are a part of the bigger loop with monomers $438 - 1 - 124$. Due to the entropic repulsion between this loop and the other two, the *oriC* and L1 are found at the poles of the cylinder with higher probabilities.

Arc-4: On comparing the localization of Arc-3 (with linear loops) and Arc-4 (with side loops), the positions of L1 and L2 loci are more delocalized for the Arc-4 architecture. This is because the smaller side loop is forced to overlap with the bigger loop and is unable to localize itself at a certain section of the cylinder. Even the data for loci R2 have a relatively flat distribution for Arc-4 as compared to the distribution for the Arc-3 architecture. Locus R3 is localized in both due to its proximity to *ter*.

Thus, we establish that we can get different polymer segments (genomic loci) to get localized in different parts of the cylinder (or the cell) by cleverly designing different polymer architectures and inducing the entropic repulsion between loops in cylindrical confinement.

Hybrid architectures: Arc-2, Arc-2-2, and Arc-9: In Fig. 7, we present the localization data for a pair of polymers with hybrid architectures, and in particular we discuss the differences between Arc-2, Arc-9, and Arc-2-2 since they have similar side loops. In Arc-2, the *oriC* is localized at the junction of the two smaller loops (with 125 monomers each) and the bigger loop with 250 monomers. Loci R1 and L1, which are part of the two smaller loops, are found closer to the pole position, and they have a similar positional probability distribution. Meanwhile, the two smaller loops also try to avoid each other while exchanging positions at the poles, and thereby have some probability of being found in the region of $0.25 - 0.75L$. Loci R2 and L2 are again closer to the point of cross-links with *oriC*, and thereby their distribution has peaks at positions close to *oriC*. Loci R3 is part of the bigger loop of the polymer and occupies the region closer to the center of cylinder.

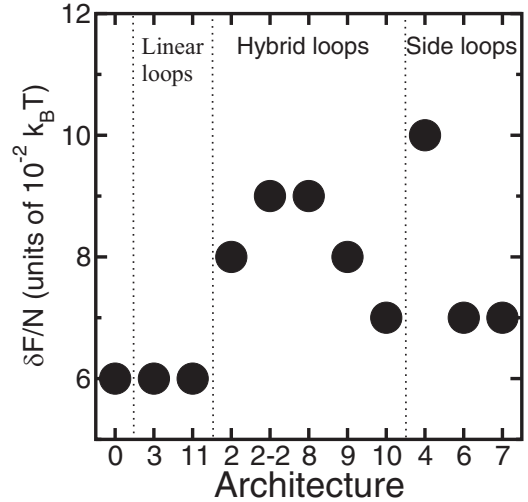


FIG. 8. Free-energy calculations from the “blob theory approach”: The figure shows the analytically estimated Helmholtz free-energy difference per monomer, $\Delta F/N$, in units of $k_B T$ between the overlapped and segregated states of the two polymers, for several polymer architectures. We assume that the free energy associated with each blob is $k_B T$ and the diameter D of the confining (open) cylinder is $10a$.

The spatial distributions of loci for a pair of polymers with Arc-9 architectures are very similar to that for Arc-2, except that for the distribution of loci R3. The bigger 250-monomer loop of Arc-2 is now divided into two smaller loops of 125 monomers each, and R3 (monomer 304) is relatively closer to the added cross-link involving monomer 312. These additional loops again repel each other in addition to the repulsion between the two (smaller) loops already present for Arc-2. As a consequence R3 has higher peaks at $0.4L$ and $0.6L$ for the Arc-9 architecture, and it also prefers to remain in the region between 0.25 and $0.75L$. The distribution for R3 is more spread out for Arc-2 architecture.

Arc-2-2 has positional distributions similar to that for Arc-2 and Arc-9, but the presence of the two smaller side loops around the central loop leads to R2 having higher probabilities near the poles, and broader distributions for R3 due to mutual repulsion between the two smaller loops near *ter*-cross-link. As a reference, we also provide the positional distributions for the ring-polymer Arc-0 architecture at the very end of Fig. 7. The positions of all the loci are highly delocalized, resulting in very broad distributions, except for the *dif-ter* loci (and R3 loci) due to the presence of the *ter*-CL.

D. The blob theory approach

We next establish that our computational results are in agreement with an analytical treatment of the free-energy difference between the segregated and unsegregated states using a blob theory approach [40–46]. Hence, we calculate the Helmholtz free-energy difference per monomer, $\Delta F/N$, between the fully overlapped and the fully segregated states of the two polymers for different architectures; refer to Fig. 8. We show that certain architectures have a larger $\Delta F/N$ and thus lead to an enhancement of entropic repulsive forces. To incorporate the effect of different architectures in free-energy

calculations, we treat each loop (of each polymer) as if it is composed of two “effective linear segments” (comprising half the number of monomers in the loop) trapped in tubes of a suitable “effective” diameter D' . The value of D' is dependent on the architecture. We provide the details of these calculations in the Appendix.

The free-energy difference between the overlapped and the segregated states of the polymers is proportional to f_{bl} . It is the free energy associated with each blob calculated with the “effective linear segment,” and it is inversely proportional to $D^{5/3}$, where D is the diameter of the cylinder of infinite length. In Fig. 8 we compare the analytically estimated $\delta F/N$, for different architectures, for a choice of $D = 10a$ and $f_{\text{bl}} = k_B T$.

We note that Arc-3 and Arc-0, both with $\delta F/N = 3 \times 10^{-2} k_B T$, are the least favorable when it comes to segregation of polymers. In Fig. 4, we note that Arc-3 and Arc-0 show similar low success rates of segregation, which is consistent with blob-theory calculations. We also note that Arc-4, Arc-2-2, and Arc-8 show the highest values of $\delta F/N$ among the investigated architectures.

However, $\delta F/N$ for Arc-4 exceeds that of Arc-8. This is not consistent with the success rates of segregation presented in Fig. 4. In computational calculations, Arc-8 shows the highest success rate of segregation. Similarly, Arc-11 shows a high success rate of segregation, which is inconsistent with relatively low $\delta F/N$ values. In general, side-looped architectures and architectures with hybrid loops have a higher $\delta F/N$ as compared to linear looped architectures and the ring polymer. We also note that Arc-4 shows a higher $\delta F/N$ as compared to Arc-3. Thus our conclusions about entropic costs arising from analytical free-energy differences between a mixed and overlapped state of two polymers are fairly consistent with previously presented simulation results in Fig. 4, though a few cases show discrepancies. We attribute this to the limitations of the effective-tube-blob theory approach. We elaborate on these limitations in the subsequent section.

We emphasize here that we have no intention to establish a causal link between free-energy calculations and the success rates of segregation. However, we indicate that there is consistency between free-energy differences between the fully overlapped and the segregated states, and the propensity to successfully segregate as obtained by computational measurements.

E. Limitations of the blob theory approach

The blob theory-based calculations that we present here rely on a few crucial approximations. Previous studies have indicated some shortcomings of this approach [47]. Our treatment considers polymers confined in an open cylinder. Moreover, the blob picture is valid only for long polymers and when the diameter D of the confining (open) cylinder is such that $D \geq 10\sigma$ [44]. Thus, the theoretical treatment assumes that the confining cylinder (and the “effective” sub-cylinders) to which the polymers are confined is sufficiently big for blob theory to hold. We use a cylinder of diameter $7a$ and length $L = 35a$ in our simulations. This leads to a few discrepancies between our computationally obtained results and our analytical results, as discussed. Be that as it may, the free-energy analysis, despite its limitations, is useful to

decipher which polymer architectures are more amenable for efficient segregation starting from a mixed state.

F. Principles of segregation and localization of polymer segments due to polymer architectures

We now establish how and why linear loops and side loops differ in terms of the organization of the constituent loops along the cylindrical long-axis as shown in Figs. 4 and 5, and thereby further our understanding. To that end, for some selected architectures we plot (i) probability distributions of the positions of the center of mass (COM) of the loops, and (ii) the number density of monomers for each loop along the cylindrical long-axis in Figs. 9 and 10, respectively.

We show in Fig. 9 that in Arc-3 (with linear loop architecture) the constituent loops show minimal spatial overlap, while for Arc-4 (with a small side loop) the two constituent loops overlap considerably as they explore different conformations. We find through our analytical calculations that a pair of polymers with Arc-4 architecture have a higher $\delta F/N$ as compared to a pair of polymers with the Arc-3 architecture.

This is also substantiated in Figs. 10(a) and 10(b), where we see that monomers of the smaller loop (marked in red) effectively reduce spatial overlap with the monomers of the bigger loop (shown in blue) for Arc-3, while the effect is reduced for Arc-4. In Arc-3 and Arc-4, the monomer density of the bigger loop (blue) is higher near midcylinder, as the *ter* monomer in the bigger loop has a cross-link with the *ter* of the other polymer. In Arc-4, the monomer densities of the smaller loop (red) have nearly the same values from the pole to the quarter position within the cylinder, whereas for Arc-3 the monomer densities decrease monotonically as one moves from the pole to midcylinder positions.

In side-looped architectures, constituent loops show more spatial overlap as compared to linearly looped ones. This is because segments belonging to different loops of a polymer occupy “effective” cylinders of smaller radii. We illustrate this through the schematic diagrams for Arc-2 (which also has side loops) presented in Appendix 2. Thus there is a higher free-energy cost of overlap of the two polymers having “side-looped” architectures. We have also shown in Fig. 4 that Arc-4 shows a higher success rate of segregation as compared to Arc-3. Moreover, Arc-3 also shows a broader distribution of D_{com} as compared to Arc-4 in Fig. 5. This is because, in a cylinder with two polymers with Arc-4 architecture, the presence of the side loops hinders the overlap of loops from two different polymers which have segregated to the two halves of the cylinder.

Furthermore, we note from Fig. 4 that Arc-11 shows a high success rate of segregation. To investigate the underlying reason, we look at the probability distributions of the positions of the COMs of each constituent loop in Arc-11 in Fig. 9. We show that all the constituent loops show significant overlap with their neighboring loop(s), though the peaks of the distributions are at distinct locations along the long axis. We attribute this to the finite length of the confining cylinder. This can also be surmised from Fig. 10(c), where the

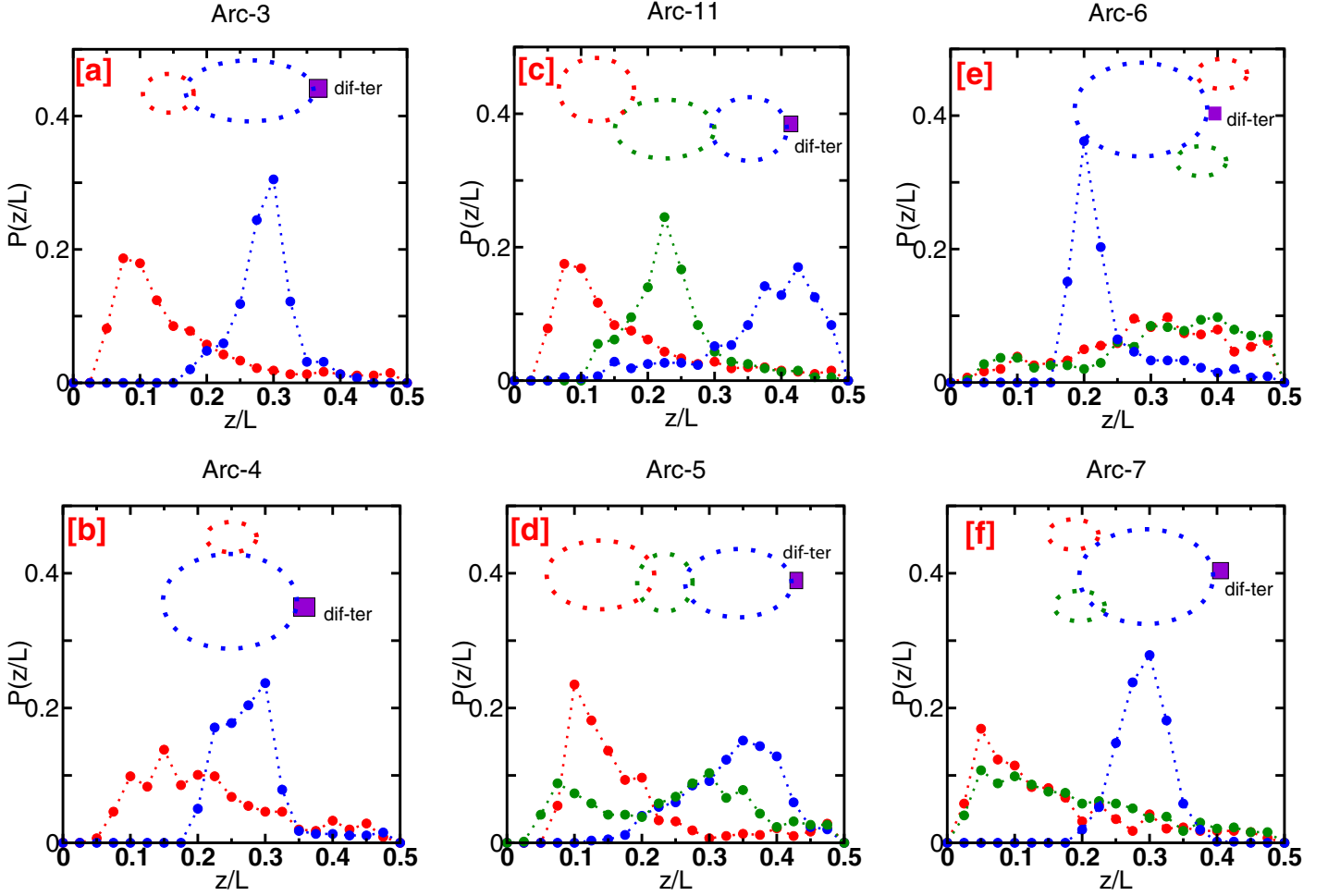


FIG. 9. The subfigures show the spatial probability distributions $P(z/L)$ of the centers of mass for loops corresponding to six architectures. The z axis is along the long axis of the cylinder and measured from one pole, and normalized by the length L of the cylinder. We also show schematic representations of the constituent loops in each subfigure. The colors of symbols in the plots correspond to the color of the particular constituent loop as shown in the schematic. Here we have two polymers conjoined at the *ter* loci. We show the data averaged over both polymers, but the range of the x -axis extends to only to $0.5L$, as the segregated polymers occupy different halves of the cylinder. The distributions have been computed from a pool of 50 independent runs for each architecture, considering only those runs that have successfully segregated.

monomers of the two loops (marked in red and blue) can be seen to largely occupy different regions of the cylinder, yet also show considerable spatial overlaps with the monomers of the central loop (marked in green). Thus, even though the configuration of the loops in Arc-11 is linear, the architecture is “effectively” a hybrid architecture having characteristics of both linear and side-looped architectures. This is the reason why Arc-11 shows high success rates of segregation as shown in Fig. 4.

Note that in our analytical calculations we had assumed that the polymers are in an open cylinder, and thus we had obtained considerably lower values of $\delta F/N$ as compared to other hybrid (and side-looped) architectures. This effect is even more pronounced (as compared to that of Arc-11) in the case of the Arc-5 architecture, where the constituent loops show even greater spatial overlap with each other. This can be confirmed with the data presented in Figs. 9(d) and 10(d). We note that the COMs of the loops (and also the monomers of

the loops) show considerable spatial overlap with each other. The degree of overlap is also higher than that of Arc-11, since the (larger) central loop in Arc-5 shows greater spatial overlap with the loops shown in red and blue, as compared to that of Arc-11. Thus, it also has a higher success rate of segregation as compared to that of Arc-11.

We had also previously mentioned that Arc-6 shows a much higher success rate of segregation as compared to Arc-7, although both of these architectures have two side loops of identical lengths (80 monomers each) attached to a bigger loop (340 monomers). Furthermore, Arc-6 shows a narrower distribution of D_{com} as compared to Arc-7 in Fig. 5. This is because in Arc-6 the two smaller additional loops are close to the *dif-ter* cross-link, while in Arc-7 the two additional loops are closer to the *oriC*.

As a consequence of their positions, in Arc-6 the two smaller loops have considerable overlap with each other and with the bigger loop, especially near the midcylinder

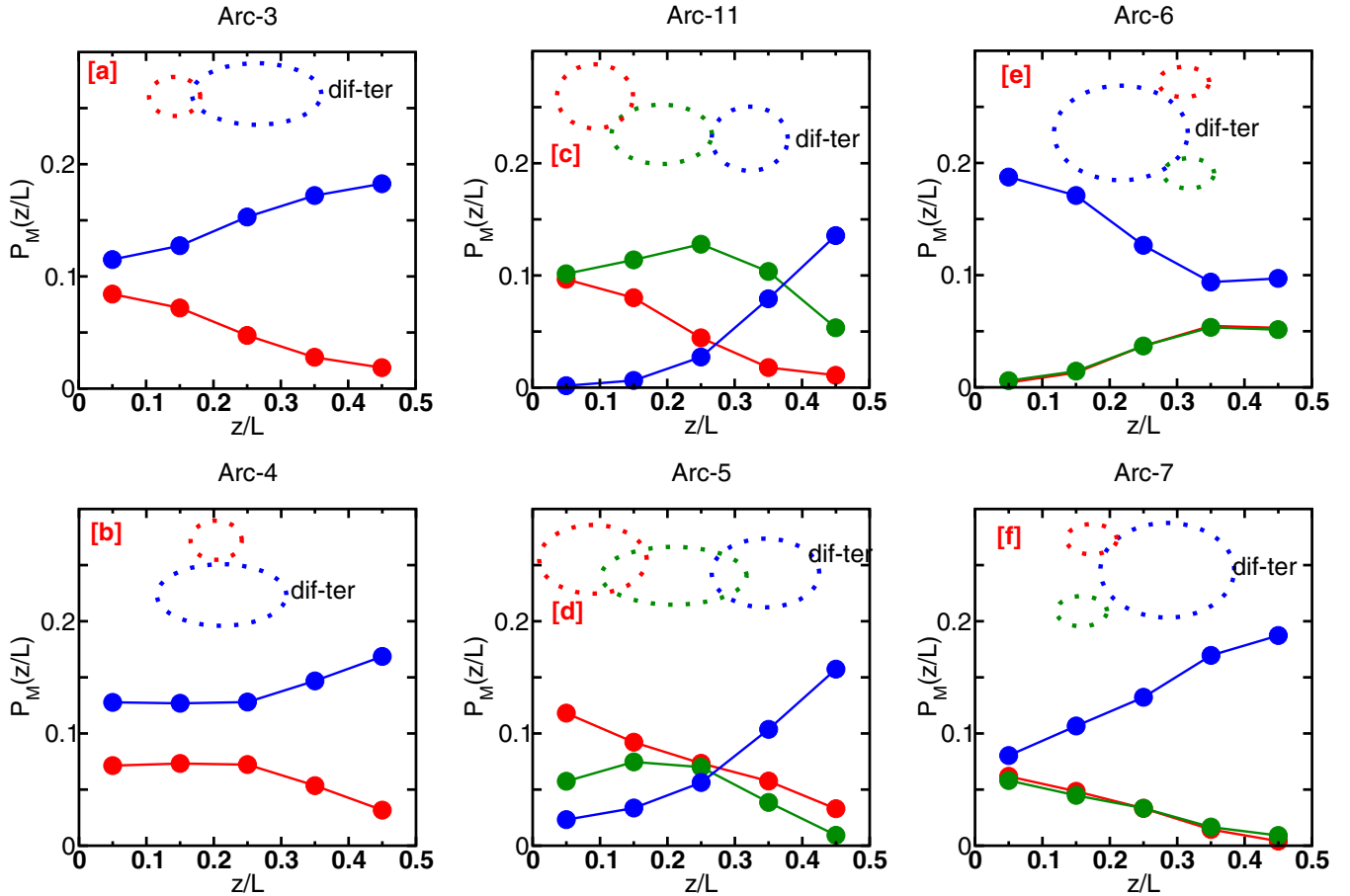


FIG. 10. The subfigures show the normalized number density $P_M(z/L)$ of monomers of different loops along the long axis \hat{z} of the cylinder, corresponding to the six architectures of Fig. 9. To calculate the monomer density, we divide the long axis into 10 different sections, we calculate the mean number of monomers belonging to a particular loop in that section, and we normalize it by the total number of monomers N ($N = 500$) in one polymer. The other figure specifications follow that of Fig. 9.

positions. On the other hand, the side loops of Arc-7 overlap considerably with each other but show relatively less overlap with the bigger loop. The monomer densities of the two smaller loops are very low near the midcell position, whereas the monomer density of the bigger loop is relatively low near the pole positions. Thus the two side loops in Arc-7 and the bigger loop mostly occupy different parts of the cylinder akin to the organization seen in linearly looped architectures. These can be confirmed from the distribution of the COMs of the constituent loops of Arc-6 and Arc-7, given in Figs. 9(e) and 9(f), as well as from data in Figs. 10(e) and 10(f).

Note that in our analytical calculations we had calculated the same $\delta F/N$ for Arc-6 and Arc-7, however the actual $\delta F/N$ is likely to be higher for Arc-6 than that of Arc-7 since there are more overlaps between the loops in Arc-6. This is the reason why Arc-6 has a much higher success rate of segregation compared to that of Arc-7.

Thus, in light of the analysis presented in this subsection, we can redefine a side-looped architecture as the kind of architecture that leads to increased spatial overlaps between the constituent monomers of the internal loops. A “linearly looped” architecture, on the other hand, shows minimal spatial

overlaps between the constituent monomers of the internal loops as they arrange themselves “linearly” along the long axis of the cylinder.

G. Summary

In summary, we conclude the following from our study on polymer architectures:

(i) For two initially overlapping polymers confined in a cylinder, we show that side-looped architectures lead to larger entropic forces of segregation. This is established analytically (as shown in Fig. 8), and it can also be inferred from our computational results presented in Figs. 4 and 5 for Arc-4 and Arc-3. Thus, Arc-4, which is a side-looped architecture, leads to higher forces of segregation compared to Arc-3, which has a linear configuration of loops.

(ii) If the loops are linearly arranged in a cylinder of finite length, then due to the finite size of the cylinder the loops may overlap and act as “side loops” in certain architectures, e.g., Arc-5 and Arc-11.

(iii) Some hybrid and side-looped architectures such as Arc-8 and Arc-6 lead to lesser fluctuations in D_{com} . Thus, spatially segregated polymers having such architectures would

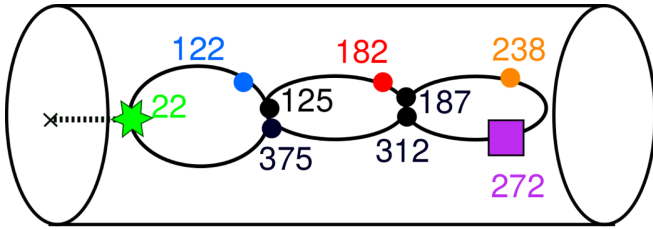


FIG. 11. The figure shows a polymer having the Arc-C architecture which is confined in a cylinder. It is similar to Arc-11, and the monomer pairs that have been cross-linked are shown in black. These monomer pairs are 125, 375 and 187, 312. In this convention, the *oriC* is monomer 22 and is tethered to the pole by a spring of spring constant $1k_B T/a^2$. The other monomers which we have shown here correspond to specific genomic loci that have been studied using FISH experiments [19]. The monomer index 122 corresponds to the locus *pilA*, the monomer index 182 corresponds to the locus *pleC*, the monomer index 238 corresponds to the locus *podJ*, and the monomer index 272 corresponds to the *ter*.

minimize partial overlaps due to thermal fluctuations. This is likely to be of importance for bacterial chromosomes where the two daughter chromosomes must segregate completely before cell-division.

(iv) Even for side-looped architectures, the segregation properties depend crucially on where the loops are located along the chain contour. This has been illustrated with the help of Arc-6 and Arc-7 in the preceding paragraphs. We

have explained why Arc-6 induces higher forces of entropic segregation as compared to Arc-7.

(v) Through the data presented in Figs. 6 and 7 we find that different architectures with additional loops lead to localization of genomic loci (monomers) at specific regions along the cylindrical axis with relatively lesser fluctuations about the mean position. However, Arc-0 (ring polymer) fails to show any such localization. Thus, one may design polymer architectures suitably to localize specific polymer segments in specific regions of the confining cylinder.

(vi) The polymer segments that are at the junction of two loops (i.e., near the cross-links) get more localized as compared to segments that are away from the junctions.

V. LOCALIZATION AND ORGANIZATION IN THE *C. CRESCENTUS* CHROMOSOME

Using the insights gained from the previous results on polymer architectures, we now design a polymer architecture called Arc-C, which is plausibly adopted by the *C. crescentus* chromosome. The polymer architecture Arc-C is shown in Fig. 11. Note that Arc-C has a linearly looped configuration similar to Arc-11, and it has just two additional CLs. To establish a correspondence with the *C. crescentus* chromosome, we first look at the spatial localization patterns of loci as have been measured in experiments for the *C. crescentus* chromosome [2,19,48].

We present in Figs. 12(a) and 12(b) the spatial probability distributions of certain loci, as obtained from experiments [19] and our simulations, respectively. We find that we reproduce

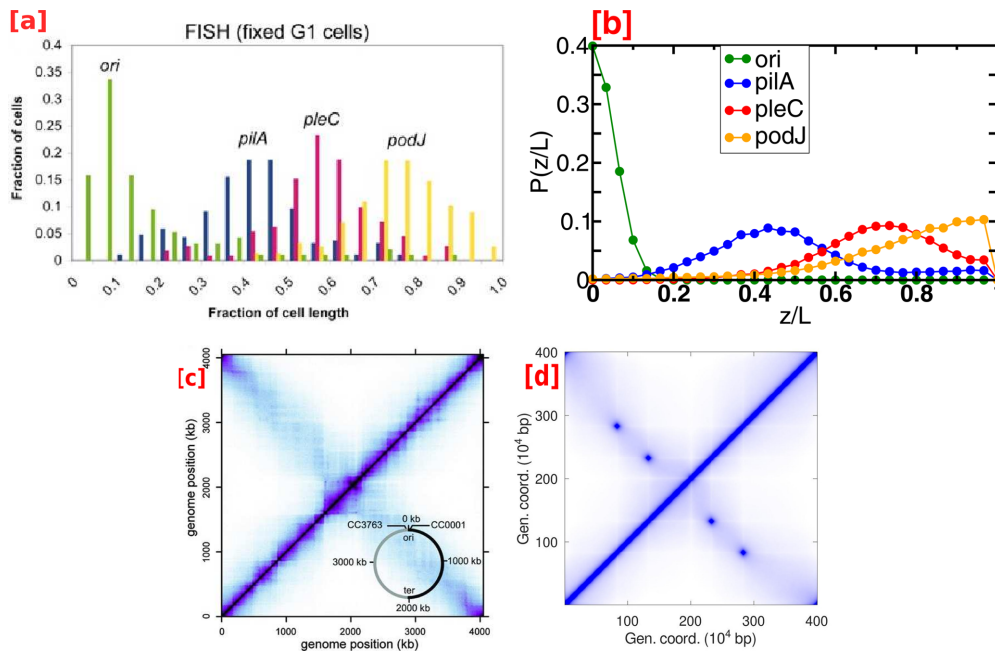


FIG. 12. Spatial organization of *C. crescentus* chromosome: Subfigures (a) and (b) show the spatial probability distributions of loci obtained from experiments and simulations, respectively. In the simulations, we use the polymer architecture Arc-C with the monomer corresponding to the *ori* tethered to the cell pole, as is the case *in vivo*. The *x*-axis has been scaled by the length of the confining cylinder. The *ori* locus remains tethered to the cell pole and therefore remains localized around the pole [2,19,48]. Furthermore, we also compare the Hi-C contact map obtained from experiments shown in (c), which is in qualitative agreement with the contact map obtained from simulations in (d), and it has the less prominent diagonal [48] characteristic of *C. crescentus* chromosome. Subfigures (a) and (c) have been reproduced from [19] [Copyright (2004) National Academy of Sciences, USA] and [48].

the localization patterns seen *in vivo* to a fair degree, despite the simplicity of our model. We find that the spatial distributions of the loci show distinct peaks. However, the positions of the peaks do not exactly match those seen *in vivo*. This is to be expected in our opinion since we employ a very minimal model. One may optimize the sizes of the loops in Arc-C to obtain an exact match with the FISH experiments, but here we only aim to establish the principles that reconcile complementary experiments conducted on the *C.crescentus* chromosome, and hence we abstain from adopting the optimization route. A previous study has already established that such localization patterns cannot be obtained from just a confined ring polymer with its *ori* tethered to the cell pole [2].

Furthermore, in Figs. 12(c) and 12(d) we show the contact maps obtained from experiments and simulations, respectively. We find that our simulated contact map is in qualitative agreement with experiments in that we obtain the other less prominent diagonal which is characteristic of *C.crescentus* Hi-C data [48]. Thus we reconcile to a far degree the experimental observations obtained from *two complementary* experiments, using our designed polymer architecture.

However, there are also a few key differences between the experimentally obtained contact map and the one obtained from simulations. The differences and the reasons for the same are listed as follows:

(i) The genomic regions corresponding to the sites of the cross-links (CLs) in the simulated contact map appear as bright blue spots along the less prominent diagonal, while such bright regions are not visible in the experimentally obtained contact map. However, we encourage the reader to zoom into these regions in the experimental contact map. Upon zooming in, one finds that the sites of the CLs do correspond to points of high probability in the experimental contact map, although they do not have the highest probabilities as in the simulated contact map.

(ii) The sites of Arc-C CLs have high probabilities in the experimental Hi-C map, however the other regions also have high contact probabilities. A question that the reader is likely to ask is, why have we not introduced other possible CLs in our model? We believe that there can be other possible CLs due to proteins that colocalize different segments of the DNA-polymer. However, we establish here that only a minimal number of long-lived CLs are required to obtain a match with the FISH data and to obtain a contact map qualitatively similar to the experimentally obtained contact map.

(iii) Next, we elaborate on why the CL sites in the simulated contact map have bright, *broad* circular patches, while the experimental Hi-C map shows relatively tiny illuminated spots at the genomic sites corresponding to the sites of the CLs used in this study. Note that in the simulations we have a resolution up to the lengthscale of a single bead ~ 8 kbp. Thus we get large bright patches, as monomers proximal to the CL sites also contribute and enlarge the size of the blue spots.

In the cell, the chromosome may have CLs (binding sites) located at specific sites over a much smaller lengthscale, viz., CLs are realized by a suitable protein having a size of \sim nm. This will change the topology over a larger lengthscale of the DNA-polymer and comparable to what is considered in this study. However, the experimentally obtained Hi-C con-

tact map has a much higher resolution of \sim kbp, and thus a protein-sized experimental cross-link is much smaller than the lengthscale of a “cross-link” in simulations. Therefore, these “cross-links” and contributions from their proximal segments would show up in the experimental Hi-C map as pointlike blue spots. Thus, in the experimental Hi-C maps, the size of the bright spot corresponding to a “cross-link” in the chromosome would be relatively tiny.

(iv) As mentioned previously, we find that the simulated contact map shows the highest probabilities of contacts at the sites of the additional cross-links. However, this is not the case for the experimental contact map, although the sites of the cross-links do show relatively high probabilities. This is because in our minimal model we assume that the additional cross-links are permanent throughout the simulation run, whereas in the *C.crescentus* chromosome these may form transiently at various points during the cell cycle. These additional “cross-links” in the *C.crescentus* chromosome may be long-lived despite forming and dissolving due to various biological processes. Furthermore, the experimental Hi-C map is calculated as an average over a large number of cells in different stages of their lifecycle, where the CLs could be dissolved in some of the chromosomes.

In the case of bacterial chromosomes such as *C.crescentus*, it is likely that there exist many other “effective cross-links” which may arise dynamically due to several proteins found *in vivo* and plectoneme super-coiling [2]. However, we propose that the cross-links we have introduced are relatively long-lived, and this is responsible for the organization of the *C.crescentus* chromosome at the lengthscales considered in our study.

As mentioned before, many past studies with more detailed models have used several cross-links to obtain a Hi-C map quantitatively similar to that of experiments [12–15,17,18]. The positions of these CLs were extracted from the Hi-C map, and the spring constants were optimized to obtain a contact map very similar to that obtained from experiments. Here we take an orthogonal approach and use just two additional CLs. Furthermore, we also show that Arc-C reconciles observations from FISH experiments. Thus, we introduce as few constraints as possible in our model and avoid introducing a large number of constraints to achieve a quantitative match with the Hi-C experimental data.

We showed previously that a particular polymer architecture localizes polymer segments (or genomic loci) of *E.coli* chromosomes [3]. Here we establish the mechanism by which this localization takes place in bacterial chromosomes, and we propose that this could be a generic method adopted by other bacterial species.

VI. DISCUSSIONS

We establish the topological mechanisms by which polymer segments of a polymer can be induced to get localized in a confined geometry by analyzing a pool of polymer architectures. This mechanism depends on the concept of tuning entropic repulsion between segments of polymers by modifying the topology and the excluded volume of monomers.

The two Arc-0 ring-polymers (each with 500 monomers) cross-linked at the *dif-ter* may also be considered as a single polymer (of 1000 monomers) with the monomers corresponding to the two *dif-ter* cross-linked. In this vein, the spatial segregation of the two polymers may be interpreted as the spatial localization of the internal loops of a 1000-monomer chain within the cylinder.

For other architectures that we have considered with additional loops, one may correspondingly imagine the system as a single polymer of 1000 monomers having many internal loops. These internal loops organize themselves differently for different architectures within the cylinder. Thus we show that by introducing strategically placed loops within a ring polymer, one can induce an “effective” repulsive interaction between particular polymer segments, which leads to specific spatial localization patterns and thereby organization of the segments.

Such entropy-driven “effective” interactions in polymers may find a host of applications where one has to design polymer systems with specific organizational properties (as in block copolymers), but without invoking explicit enthalpic interactions. We also establish the principle by which modified polymer architectures lead to an enhancement of the entropic repulsion between overlapping polymers, and thereby aid the segregation process. We show this by analytically estimating the free-energy difference between overlapped and segregated states for several polymer architectures using the blob theory approach [44].

These modified architectures may arise in bacterial chromosomes to accomplish biological functions [16], but they may also lead to the enhancement of the entropic forces of segregation. We also show that the release of topological constraints plays a crucial role in the enhancement of the segregation process and also results in a significant increase in the success rates of segregation. Furthermore, several experimental results have shown previously that chromosomal loci show specific localization patterns in bacterial chromosomes [7,22]. Thus we show here that such localization patterns observed for *C.crescentus* chromosomes are consistent with those obtained with polymer architecture Arc-C. Previously, we established that architecture Arc-2-2 reconciles spatiotemporal localization patterns seen in experiments for the *E.coli* bacterial chromosome [3]. Thereby, this current manuscript further strengthens the thesis that bacterial chromosomes employ this generic principle of entropy-based organization of polymeric segments, namely to segregate and organize itself within the cell.

However, as we have established here even for synthetic polymers in confinement, which do not have a topological constraint release mechanism, the loops (and consequently polymer segments) will organize themselves using its internal loop topology for cases in which segregation has been successful. The corresponding data are in the SI (Figs. S4–S9) [33]. Note that it is possible (and likely) that if we run much longer simulations, then all the initially overlapping polymers would spatially segregate for runs with a constraint release mechanism. This is also likely to be true for the case when we start out with nonconcatenated polymers without a constraint release mechanism in place, though the dynamics will be slower because release of topological con-

straints may take more time. The mean value of N_{MCS} , the number of MCSs required for segregation for particular architectures, would increase if we wait for polymers in all independent runs to successfully segregate. Thus the mean N_{MCS} in that case would show greater differences across architectures than what we have presented in this paper. In this manuscript, we focus instead on the success rates of segregation since the simulation times required for complete segregation for all architectures are computationally inaccessible. But, if we had 100% success rates of segregation, then N_{MCS} would show much larger variation in values. Thus these two quantities are complementary to each other in a sense, and either can be used to reach the conclusions we have presented.

Future advances in nanotechnology may rely on the principles outlined here of strategically designing polymer architectures to induce localization of certain polymer segments. One can envisage applications in nanomedicines which may require spatial localization of pharmaceutical cargo in confined environments [49,50]. In the past decade there have been several experimental methods [51] developed to design well-defined ring polymers, and moreover derive more complex multicyclic topologies analogous to what we have used. This allows for exploration of their properties arising from their topology and thereby finding new potential applications as they can be self-assembled into hierarchical macromolecular architectures at larger scales [52] and more unique dynamical properties [53]. More fundamentally, the approach of tuning entropic interactions between polymer segments via polymer architectures could also be employed by researchers from diverse backgrounds to obtain microphase separation of polymeric mixtures induced solely due to entropic considerations without having to invoke enthalpic interactions between the constituent polymers.

ACKNOWLEDGMENTS

A.C., with DST-SERB identification SQUID-1973-AC-4067, acknowledges funding by DST-India, project MTR/2019/000078 and CRG/2021/007824. A.C. also acknowledges discussions in meetings organized by ICTS, Bangalore, India.

D.M. and A.C. designed the work and wrote the manuscript. S.P. and D.M. performed simulations and analyzed data. D.M. did the analytic blob theory calculations and also established the biological relevance of our studies.

The authors declare no competing financial interest.

APPENDIX: FREE ENERGY OF POLYMERS OF DIFFERENT TOPOLOGIES IN A CYLINDER OF DIAMETER D

1. Arc-0: Free-energy difference δF between the overlapped and the segregated configurations

a. Free energy F_{seg} of two segregated ring polymers in an infinite cylinder

To calculate the Helmholtz free energy F_{seg} for two segregated ring polymers, conjoined at the *ter* and confined in a cylinder of diameter D , we use the blob theory approach,

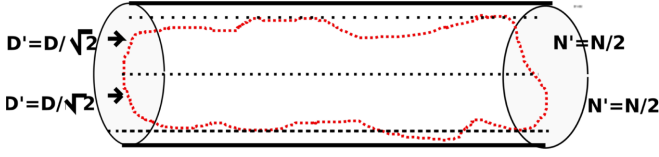


FIG. 13. A schematic representation of a single ring polymer with $N = 500$ monomers is shown. Each arm of the ring polymer from monomer number 1 to 250 with $N' = N/2 = 250$ monomers can be visualized as a linear segment constrained in an effective tube of diameter $D' \approx D/\sqrt{2}$. We assume that the two overlapping segments occupy equal volumes per unit length (L'), but the sum of the volumes of the two smaller cylinders is equal to the volume of the bigger cylinder, viz., $\pi(D')^2L' + \pi(D')^2L' = \pi D^2L'$, thus $D' = D/\sqrt{2}$.

which calculates the free energy of blobs of polymers in confinement in an infinitely long cylinder of diameter D . We calculate the free energy corresponding to just one confined ring polymer given by F_{conf} . The free energy of two segregated ring polymers is given by

$$F_{\text{seg}} = 2F_{\text{conf}}. \quad (\text{A1})$$

To calculate F_{conf} , we first assume that each linear segment containing $N' = N/2$ monomers (see Fig. 13) is constrained to a tube of an effective diameter of $D' \approx D/\sqrt{2}$ [44]. This choice of the diameter D' of the effective tubes ensures that the combined volume of the two tubes is equal to the volume of the cylinder of diameter D .

A segment (blob) of a self-avoiding polymer chain with g monomers spans diameter D' such that $D' = a \times g^{3/5}$ monomers. Thus the total number of monomers in each “blob” is given by

$$g = (D/\sqrt{2})^{5/3}, \quad (\text{A2})$$

and the total number of self-avoiding blobs within a cylinder, for two linear chains of N' monomers, is therefore given by

$$n_{\text{bl}} = 2 \times (N'/g) = 2 \times \frac{N}{2} \times (\sqrt{2}/D)^{5/3}. \quad (\text{A3})$$

If the free energy associated with each blob is given by f_{bl} (later taken $\approx k_B T$), then the free energy of two ring polymers is $2n_{\text{bl}}f_{\text{bl}}$ if they are not overlapping, i.e., in the segregated state. Thus the free energy of two ring polymers that are segregated in an infinite cylinder F_{seg} is given by

$$F_{\text{seg}} = 2F_{\text{conf}} = 2 \times \frac{N}{D^{5/3}} \times 2^{5/6} \times f_{\text{bl}}. \quad (\text{A4})$$

b. Free energy F_{ov} of two ring polymers in overlapped state in an infinite cylinder

To calculate the Helmholtz free energy F_{ov} for two overlapping ring polymers (conjoined at the ter), we assume that each arm of a single ring polymer containing $N' = N/2 = 250$ monomers occupies an effective tube of diameter $D' = D/2$. Note that there are four such linear arms since there are two overlapping ring polymers. The cross-sectional area of the four tubes (each containing a polymer arm) remains $4 \times \pi(D')^2 = \pi D^2$. Thus the total number of monomers in

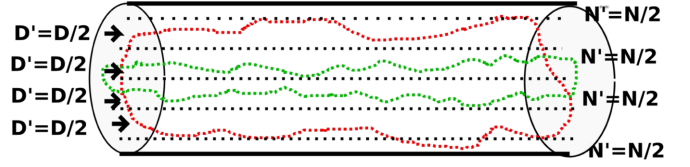


FIG. 14. A schematic representation of two overlapping ring polymers (shown in red and green) where each arm can be visualized as a linear segment constrained in an effective tube of diameter $D' \approx D/2$.

each “blob” is given by

$$g = (D/2)^{5/3}, \quad (\text{A5})$$

and the total number of blobs for four polymer arms is therefore given by

$$n_{\text{bl}} = 4 \times (N'/g) = 4 \times \frac{N}{2} \times (2/D)^{5/3}. \quad (\text{A6})$$

If the free energy associated with each blob is given by f_{bl} , then the free energy of the overlapped state F_{ov} is given by

$$F_{\text{ov}} = 2N \times (2/D)^{5/3} \times f_{\text{bl}}. \quad (\text{A7})$$

Thus the free-energy difference per monomer between the overlapped and the segregated state for two Arc-0 (ring polymers) in a cylinder of diameter D is given by

$$\delta F/N = (F_{\text{ov}} - F_{\text{seg}})/N = 2.78 f_{\text{bl}}/D^{5/3}. \quad (\text{A8})$$

2. δF between the overlapped and the segregated states of two polymers with Arc-2 architecture

A polymer with the Arc-2 architecture has two loops of 125 monomers each in a chain of 500 monomers. Thus there are $N/4$ monomers in each of the smaller loops of a polymer having Arc-2 architecture, while the bigger loop has $N/2$ monomers; refer to Fig. 3 for the schematic.

a. Free energy F_{seg} of two Arc-2 polymers in segregated state in an infinite cylinder

To calculate the Helmholtz free energy for two segregated polymers (conjoined at the ter) of architecture Arc-2 using the blob theory approach, we calculate the free energy of just one confined polymer, F_{conf} , in an infinitely long cylinder. The free energy of the two segregated ring polymers is $F_{\text{seg}} = 2F_{\text{conf}}$.

To calculate F_{conf} , we assume that F_{conf} is given by the sum of free energies in section I and section II: $F_{\text{conf}} = F_{\text{I}} + F_{\text{II}}$, where F_{I} and F_{II} denote the contributions to the free energy from sections I and II of the cylinder; refer to the top subfigure of Fig. 14.

(i) In polymer segments occupying section I, each linear segment of $N' = N/8$ monomers (the number of monomers in one of the smaller loops is $N/4$) is constrained in a tube of an effective diameter of $D' \approx D/2$. The value of D' can be calculated considering that there are four cylinders of diameter D' . The sum of the volume of the four cylinders is equal to that of a cylinder with diameter D . Thus the number of monomers in

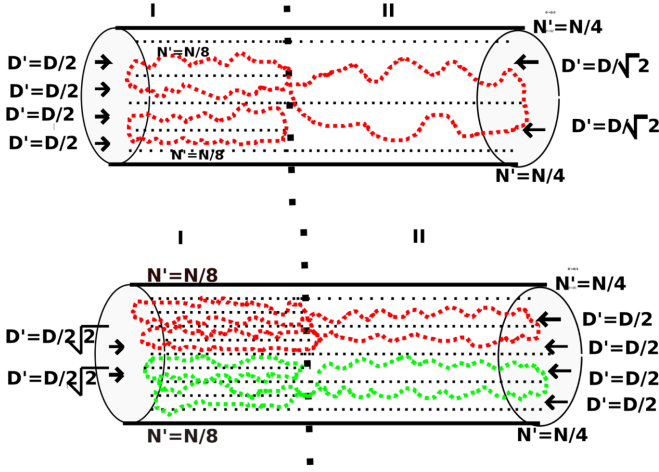


FIG. 15. The top subfigure shows a schematic representation of a single polymer in the Arc-2 configuration confined in a cylinder of diameter D . The cylinder can be divided into two sections: section I containing the two smaller loops, and section II containing the larger loop with $N/2$ monomers. The larger loop, which itself is a ring polymer with $N/2$ monomers, can be visualized as two linear overlapping linear chain segments with $N/4$ monomers in each segment. Each linear segment of $N' = N/4$ monomers is confined in an effective tube of diameter $D' \approx D/\sqrt{2}$. In section I, there are the two smaller loops (ring polymers) with $N/4$ monomers each. Each loop can be thought of as containing two linear segments with $N/8$ monomers, each occupying effective tubes of diameter $D' \approx D/2$. The subfigure at the bottom shows a schematic representation of two overlapping Arc-2 polymers (shown in red and green) where the bigger loops of section II can be conceptualized as four linear polymer segments, each constrained in an effective tube of diameter $D' \approx D/2$. In section I, there are eight overlapping linear segments, each confined in cylindrical tubes of $D/(2\sqrt{2})$. Each smaller loop as $N/4$ monomers, hence each linear segment has $N/8$ monomers.

each “blob” is given by

$$g = (D/2)^{5/3}, \quad (\text{A9})$$

and the total number of blobs from four linear chains with $N/8$ monomers is given by

$$n_{\text{bl}} = 4 \times \frac{N}{8} \times (2/D)^{5/3}. \quad (\text{A10})$$

If the free energy associated with each blob is given by f_{bl} , then the free energy F_I is given by

$$F_I = (N/2)/D^{5/3} \times 2^{5/3} f_{\text{bl}}. \quad (\text{A11})$$

(ii) In section II, each linear segment of $N/4$ monomers is constrained in a tube of an effective diameter of $D' \approx D/\sqrt{2}$. The number of monomers in each “blob” is

$$g = (D/\sqrt{2})^{5/3} \quad (\text{A12})$$

and the total number of blobs from two chains each with $(N/4)$ monomers is

$$n_{\text{bl}} = 2 \times \frac{N}{4} \times (\sqrt{2}/D)^{5/3}. \quad (\text{A13})$$

If the free energy associated with each blob is given by f_{bl} , then $F_{\text{II}} = n_{\text{bl}} f_{\text{bl}}$:

$$F_{\text{II}} = 2 \times \frac{N}{2} \times (\sqrt{2}/D)^{5/3} \times f_{\text{bl}}. \quad (\text{A14})$$

(iii) So finally, for two segregated Arc-2 polymers that are next to each other in an infinite cylinder of diameter D ,

$$F_{\text{seg}} = 2F_{\text{conf}} = 2(F_I + F_{\text{II}}). \quad (\text{A15})$$

b. Free energy F_{ov} of two Arc-2 polymers in an overlapped state in an infinite cylinder

To calculate the Helmholtz free energy using the blob theory approach, for two overlapped polymers (conjoined at the ter) of architecture Arc-2, we once again employ the same approach as before. Thus, to calculate F_{ov} we first assume that F_{ov} is given by $F_{\text{ov}} = F_I + F_{\text{II}}$, where F_I and F_{II} denote the contributions to the free energy from sections I and II, as shown in the bottom subfigure of Fig. 15.

(i) In section I, each linear segment of $N/8$ monomers is constrained in a tube of an effective diameter of $D' \approx D/2\sqrt{2}$. Thus the number of monomers in each “blob” is given by

$$g = (D/2\sqrt{2})^{5/3}, \quad (\text{A16})$$

and the total number of blobs is therefore

$$n_{\text{bl}} = 8 \times N/8 \times (2\sqrt{2}/D)^{5/3}/D^{5/3}. \quad (\text{A17})$$

If the free energy associated with each blob is given by f_{bl} , then the free energy F_I is given by

$$F_I = N \times (2\sqrt{2})^{5/3}/D^{5/3} f_{\text{bl}}. \quad (\text{A18})$$

(ii) Refer to the subfigure at the bottom of Fig. 15. In section II of the cylinder in the bottom subfigure, each linear segment of $N/4$ monomers is constrained in a tube of an effective diameter of $D' \approx D/2$. Thus the number of monomers in each “blob” is given by

$$g = (D/2)^{5/3} \quad (\text{A19})$$

and the total number of blobs is therefore given by

$$n_{\text{bl}} = 4 \times N/4 \times 2^{5/3}/D^{5/3}. \quad (\text{A20})$$

If the free energy associated with each blob is given by f_{bl} , then the free energy F_{II} is given by

$$F_{\text{II}} = N \times 2^{5/3}/D^{5/3} f_{\text{bl}}. \quad (\text{A21})$$

Thus,

$$F_{\text{ov}} = F_I + F_{\text{II}}. \quad (\text{A22})$$

Thus the free-energy difference per monomer, δF , between the overlapped and the segregated states of a pair of polymers with architecture Arc-2 is

$$\delta F/N = (F_{\text{ov}} - F_{\text{seg}})/N = 3.87 f_{\text{bl}}/D^{5/3}. \quad (\text{A23})$$

Thus in this way we can calculate $\delta F/N$ for each polymer architecture using the blob theory approach in which each loop is treated as linear chains trapped in an effective tube.

Other possible overlapping arrangements of two Arc-2 polymers in confinement: We have assumed a particular configuration of the “Arc-2” polymer where the two smaller loops occupy section I and the bigger loop occupies section II of the

TABLE II. This table indicates the $\delta F/N$ corresponding to each polymer architecture, except Arc-5. This is because Arc-5 has a “nested-loop”-like architecture that cannot be treated by the simplistic blob theory approach. In Fig. 7 of the main manuscript, we present $\delta F/N$ for each polymer architecture for an arbitrary set of parameters: $D = 10a$ and $f_{bl} = k_B T$.

Architecture	$\delta F/N$
Arc-0	$2.78 f_{bl}/D^{5/3}$
Arc-2	$3.87 f_{bl}/D^{5/3}$
Arc-2-2	$4.0 f_{bl}/D^{5/3}$
Arc-3	$2.78 f_{bl}/D^{5/3}$
Arc-4	$4.90 f_{bl}/D^{5/3}$
Arc-6	$3.30 f_{bl}/D^{5/3}$
Arc-7	$3.30 f_{bl}/D^{5/3}$
Arc-8	$4.36 f_{bl}/D^{5/3}$
Arc-9	$3.84 f_{bl}/D^{5/3}$
Arc-10	$3.23 f_{bl}/D^{5/3}$
Arc-11	$2.85 f_{bl}/D^{5/3}$

cylinder, both in the overlapped and the segregated scenarios. To rule out the possibility that (i) one smaller loop occupies section I, and the other smaller loop overlaps with the bigger loop in section II of the cylinder, we have calculated (using the method outlined above) that the free energy for confinement for such a configuration is higher than the configuration discussed in detail above. (ii) Other possible configurations, such as that of all loops occupying the same cylinder half, also have higher values of free energy. (iii) For one small loop occupying the same half as one of the bigger loops, the free energy of confinement (F_{conf}) is increased by $0.3N/D^{5/3} f_{bl}$.

Similarly, we do this for all our calculations pertaining to different architectures.

3. $\delta F/N$ corresponding to all polymer architectures

In Table II we present the analytically calculated $\delta F/N$ for different architectures using the methods outlined in the previous sections.

- [1] S. Jun and A. Wright, Entropy as the driver of chromosome segregation, *Nat. Rev. Microbiol.* **8**, 600 (2010).
- [2] J. J. B. Messelink, M. C. F. van Teeseling, J. Janssen, M. Thanbichler, and C. P. Brodersz, Learning the distribution of single-cell chromosome conformations in bacteria reveals emergent order across genomic scales, *Nat. Commun.* **12**, 1963 (2021).
- [3] D. Mitra, S. Pande, and A. Chatterji, Polymer architecture orchestrates the segregation and spatial organization of replicating *E. coli* chromosomes in slow growth, *Soft Matter* **18**, 5615 (2022).
- [4] A. Hofmann, J. Mäkelä, D. J. Sherratt, D. Heermann, and S. M. Murray, Self-organised segregation of bacterial chromosomal origins, *eLife* **8**, e46564 (2019).
- [5] V. S. Lioy, I. Junier, and F. Boccard, Multiscale dynamic structuring of bacterial chromosomes, *Annu. Rev. Microbiol.* **75**, 541 (2021).
- [6] J. Mäkelä and D. J. Sherratt, Organization of the escherichia coli chromosome by a MukBEF axial core, *Mol. Cell* **78**, 250 (2020).
- [7] J. A. Cass, N. J. Kuwada, B. Traxler, and P. A. Wiggins, Escherichia coli chromosomal loci segregate from midcell with universal dynamics, *Biophys. J.* **110**, 2597 (2016).
- [8] B. Youngren, H. J. Nielsen, S. Jun, and S. Austin, The multifork escherichia coli chromosome is a self-duplicating, and self-segregating thermodynamic ring polymer, *Genes Dev.* **28**, 71 (2014).
- [9] D. Chaudhuri and B. M. Mulder, Spontaneous Helicity of a Polymer with Side Loops Confined to a Cylinder, *Phys. Rev. Lett.* **108**, 268305 (2012).
- [10] S. Jun and B. Mulder, Entropy-driven spatial organization of highly confined polymers: Lessons for the bacterial chromosome, *Proc. Natl. Acad. Sci. (USA)* **103**, 12388 (2006).
- [11] J. Pelletier, K. Halvorsen, B.-Y. Ha, R. Paparcone, S. J. Sandler, C. L. Woldringh, W. P. Wong, and S. Jun, Physical manipulation of the escherichia coli chromosome reveals its soft nature, *Proc. Natl. Acad. Sci. (USA)* **109**, E2649 (2012).
- [12] T. Agarwal, G. P. Manjunath, F. Habib, P. L. Vaddavalli, and A. Chatterji, Role of special cross-links in structure formation of bacterial DNA polymer, *J. Phys.: Condens. Matter* **30**, 034003 (2018).
- [13] T. Agarwal, G. P. Manjunath, F. Habib, and A. Chatterji, Origin of spatial organization of DNA-polymer in bacterial chromosomes, *Europhys. Lett.* **121**, 18004 (2018).
- [14] T. Agarwal, G. P. Manjunath, F. Habib, and A. Chatterji, Bacterial chromosome organization. I. Crucial role of release of topological constraints, and molecular crowders, *J. Chem. Phys.* **150**, 144908 (2019).
- [15] T. Agarwal, G. P. Manjunath, F. Habib, and A. Chatterji, Bacterial chromosome organization. II. Few special cross-links, cell confinement, and molecular crowders play the pivotal roles, *J. Chem. Phys.* **150**, 144909 (2019).
- [16] M. Fritsche, S. Li, D. W. Heermann, and P. A. Wiggins, A model for Escherichia coli chromosome packaging supports transcription factor-induced DNA domain formation, *Nucl. Acids Res.* **40**, 972 (2012).
- [17] A. Wasim, A. Gupta, and J. Mondal, A Hi-C data-integrated model elucidates *E. coli* chromosome’s multiscale organization at various replication stages, *Nucl. Acids Res.* **49**, 3077 (2021).
- [18] M. Nicodemi and A. Pombo, Models of chromosome structure, *Curr. Opin. Cell Biol.* **28**, 90 (2014).
- [19] P. H. Viollier, M. Thanbichler, P. T. McGrath, L. West, M. Meewan, H. H. McAdams, and L. Shapiro, Rapid, and sequential movement of individual chromosomal loci to specific subcellular locations during bacterial DNA replication, *Proc. Natl. Acad. Sci. (USA)* **101**, 9257 (2004).
- [20] S. Adachi, M. Kohiyama, T. Onogi, and S. Hiraga, Localization of replication forks in wild-type, and mukB mutant cells of escherichia coli, *Mol. Genet. Genomics* **274**, 264 (2005).

- [21] S. Duigou and F. Boccard, Long range chromosome organization in *Escherichia coli*: The position of the replication origin defines the non-structured regions, and the right, and left macrodomains, *PLoS Genet.* **13**, e1006758 (2017).
- [22] A. Badrinarayanan, T. B. K. Le, and M. T. Laub, Bacterial chromosome organization, and segregation, *Annu. Rev. Cell Dev. Biol.* **31**, 171 (2015).
- [23] X. Wang, X. Liu, C. Possoz, and D. J. Sherratt, The two *Escherichia coli* chromosome arms locate to separate cell halves, *Genes Dev.* **20**, 1727 (2006).
- [24] A. Vologodskii, Disentangling DNA molecules, *Phys. Life Rev.* **18**, 118 (2016).
- [25] J. L. Sikorav and G. Jannink, Kinetics of chromosome condensation in the presence of topoisomerases: a phantom chain model, *Biophys. J.* **66**, 827 (1994).
- [26] C. Micheletti, D. Marenduzzo, and E. Orlandini, Polymers with spatial or topological constraints: Theoretical, and computational results, *Phys. Rep.* **504**, 1 (2011).
- [27] V. S. Liroy, A. Cournac, M. Marbouty, S. Duigou, J. Mozziconacci, O. Espéli, F. Boccard, and R. Koszul, Multiscale structuring of the *E. coli* chromosome by nucleoid-associated, and condensin proteins, *Cell* **172**, 771 (2018).
- [28] S. J. Messerschmidt and T. Waldminghaus, Dynamic organization: Chromosome domains in *Escherichia coli*, *J. Mol. Microbiol. Biotechnol.* **24**, 301 (2014).
- [29] M. Valens, S. Penaud, M. Rossignol, F. Cornet, and F. Boccard, Macrodomain organization of the *Escherichia coli* chromosome, *EMBO J.* **23**, 4330 (2004).
- [30] A. Hofmann and D. W. Heermann, The role of loops on the order of eukaryotes, and prokaryotes, *FEBS Lett.* **589**, 2958 (2015).
- [31] F. Wu, P. Swain, L. Kuijpers, X. Zheng, K. Felner, M. Guurink, J. Solari, S. Jun, T. S. Shimizu, D. Chaudhuri, B. Mulder, and C. Dekker, Cell boundary confinement sets the size, and position of the *E. coli* chromosome, *Curr. Biol.* **29**, 2131 (2019).
- [32] F. J. Trueba and C. L. Woldringh, Changes in cell diameter during the division cycle of *Escherichia coli*, *J. Bacteriol.* **142**, 869 (1980).
- [33] See Supplemental Material at <http://link.aps.org/supplemental/10.1103/PhysRevE.106.054502> for additional information.
- [34] K. Kikuchi, M. Yoshida, T. Maekawa, and H. Watanabe, Metropolis Monte Carlo method as a numerical technique to solve the Fokker-Planck equation, *Chem. Phys. Lett.* **185**, 335 (1991).
- [35] F. Romano, C. De Michele, D. Marenduzzo, and E. Sanz, Monte Carlo, and event-driven dynamics of Brownian particles with orientational degrees of freedom, *J. Chem. Phys.* **135**, 124106 (2011).
- [36] A. Singh, A. Singh, and A. Chakraborti, Effect of bond-disorder on the phase-separation kinetics of binary mixtures: A Monte Carlo simulation study, *J. Chem. Phys.* **147**, 124902 (2017).
- [37] K. Binder and W. Paul, Monte Carlo simulations of polymer dynamics: Recent advances, *J. Polym. Sci. Part B* **35**, 1 (1997).
- [38] S. C. Glotzer, D. Stauffer, and N. Jan, Monte Carlo Simulations of Phase Separation in Chemically Reactive Binary Mixtures, *Phys. Rev. Lett.* **72**, 4109 (1994).
- [39] S. Jun, D. Thirumalai, and B.-Y. Ha, Compression and Stretching of a Self-Avoiding Chain in Cylindrical Nanopores, *Phys. Rev. Lett.* **101**, 138101 (2008).
- [40] Y. Jung, C. Jeon, J. Kim, H. Jeong, S. Jun, and B.-Y. Ha, Ring polymers as model bacterial chromosomes: Confinement, chain topology, single chain statistics, and how they interact, *Soft Matter* **8**, 2095 (2012).
- [41] Y. Jung, J. Kim, S. Jun, and B.-Y. Ha, Intrachain ordering, and segregation of polymers under confinement, *Macromolecules* **45**, 3256 (2012).
- [42] E. Minina and A. Arnold, Induction of entropic segregation: the first step is the hardest, *Soft Matter* **10**, 5836 (2014).
- [43] E. Minina and A. Arnold, Entropic segregation of ring polymers in cylindrical confinement, *Macromolecules* **48**, 4998 (2015).
- [44] B.-Y. Ha and Y. Jung, Polymers under confinement: Single polymers, how they interact, and as model chromosomes, *Soft Matter* **11**, 2333 (2015).
- [45] S. Jun, A. Arnold, and B.-Y. Ha, Confined Space and Effective Interactions of Multiple Self-Avoiding Chains, *Phys. Rev. Lett.* **98**, 128303 (2007).
- [46] A. Arnold and S. Jun, Time scale of entropic segregation of flexible polymers in confinement: Implications for chromosome segregation in filamentous bacteria, *Phys. Rev. E* **76**, 031901 (2007).
- [47] J. M. Polson and D. R.-M. Kerry, Segregation of polymers under cylindrical confinement: effects of polymer topology, and crowding, *Soft Matter* **14**, 6360 (2018).
- [48] T. B. K. Le, M. V. Imakaev, L. A. Mirny, and M. T. Laub, High-resolution mapping of the spatial organization of a bacterial chromosome, *Science* **342**, 731 (2013).
- [49] K. Ulbrich, K. Holá, V. Šubr, A. Bakandritsos, J. Tuček, and R. Zbořil, Targeted drug delivery with polymers, and magnetic nanoparticles: Covalent, and noncovalent approaches, release control, and clinical studies, *Chem. Rev.* **116**, 5338 (2016).
- [50] Y. K. Sung and S. W. Kim, Recent advances in polymeric drug delivery systems, *Biomater. Res.* **24**, 12 (2020).
- [51] R. Liénard, J. De Winter, and O. Coulembier, Cyclic polymers: Advances in their synthesis, properties, and biomedical applications, *J. Polym. Sci.* **58**, 1481 (2020).
- [52] C. Chen and T. Weil, Cyclic polymers: synthesis, characteristics, and emerging applications, *Nanoscale Horizons* **7**, 1121 (2022).
- [53] Y. Li, Y. Li, E. Prince, J. I. Weitz, S. Panyukov, A. Ramachandran, M. Rubinstein, and E. Kumacheva, Fibrous hydrogels under biaxial confinement, *Nat. Commun.* **13**, 3264 (2022).